From Department of Molecular Medicine and Surgery
Karolinska Institutet, Stockholm, Sweden

ADVANCED ELECTROCARDIOGRAPHY IN MYOCARDIAL ELECTRICAL REMODELING – INSIGHTS FROM CARDIOVASCULAR MAGNETIC RESONANCE IMAGING

Maren Maanja

Karolinska Institutet

Stockholm 2020

Cover:

A normal conventional 12-lead ECG from a patient with left ventricular hypertrophy. The columns show leads I-III, leads aVR, aVL, and aVF, leads V1-V3, and leads V4-V6, respectively. Figure modified from *Study I*.

Back cover photo by Marilia Bognandi.

Published by Karolinska Institutet.
Printed by E-Print AB 2020

ISBN 978-91 -7831-596-3

Advanced electrocardiography in myocardial electrical remodeling – insights from cardiovascular magnetic resonance imaging

THESIS FOR DOCTORAL DEGREE (Ph.D.)

By

Maren Maanja, MD

Principal Supervisor:
Martin Ugander, MD, PhD
Karolinska Institutet
Department of Molecular Medicine and Surgery
Unit of Clinical Physiology

Co-supervisors:
Todd T. Schlegel, MD
Karolinska Institutet
Department of Molecular Medicine and Surgery
Unit of Clinical Physiology

Björn Wieslander, MD, PhD
Karolinska Institutet
Department of Molecular Medicine and Surgery
Unit of Clinical Physiology

Andreas Sigfridsson, PhD
Karolinska Institutet
Department of Molecular Medicine and Surgery
Unit of Clinical Physiology

Opponent:
Peter A. Noseworthy, MD
Mayo Clinic
Department of Cardiovascular Medicine

Examination Board:
Sverker Jern, MD, PhD
Göteborgs Universitet
Department of Medicine

Elin Trägårdh, MD, PhD
Lunds Universitet
Department of Clinical Physiology and Nuclear Medicine

Lennart Bergfeldt, MD, PhD
Göteborgs Universitet
Department of Medicine

"Two roads diverged in a wood, and I–

I took the one less traveled by"

– Robert Frost

POPULAR SCIENCE SUMMARY

The heart is arguably our most beloved organ. It is essential for life, and keeps the blood pumping in our bodies so that life can be enjoyed – in the setting of a healthy heart. Heart disease is a major cause of death and suffering in the world. Heart disease is a broad term including diseases that affect the heart itself, as well as diseases that also affect the blood vessels, including high blood pressure. For someone diagnosed with heart disease, it may be of interest to know what the future holds. To answer such questions, we need to examine the heart. One way of doing this is by cracking the chest open and looking at the exposed heart. Fortunately, safer options exist, and are recommended.

Before each heartbeat, an electrical impulse that can be described as a chain reaction of firework bursts spreads through the heart. This electrical impulse results in the heart squeezing together, flushing the blood from the heart out through the blood vessels to the rest of the body´s organs. The electrical impulses of the heart can be recorded with an electrocardiography (ECG) machine by placing electrodes on the surface of the chest. In healthy hearts, the electrical firework patterns look fairly similar, but in heart disease the firework pattern may change. The ECG is a fast, accessible, and commonly used tool for diagnosing heart disease. However, it does not perfectly detect heart disease in all sick patients. That is why this thesis evaluated and developed the use of advanced ECG methods, whereby the electrical impulses – the firework pattern – were analyzed in a more technically advanced way than is typically done in a conventional ECG. The results of this thesis show that when using advanced ECG, heart disease can be confirmed or dismissed more accurately than otherwise.

To see beyond the heart's fireworks and into the structure and function of the heart, the work in this thesis used magnetic resonance imaging (MRI). MRI shows how the heart is moving and pumping, and also provides information about the heart muscle that otherwise can only be detected by viewing tissue samples in a microscope. Thus, MRI provides information about the heart that is close to that which could be obtained by cracking the chest open. The research in this thesis used both advanced ECG and MRI to evaluate the heart. With these tools, this thesis has found improved ways of detecting and diagnosing heart disease in patients using ECG, and new ways of predicting the risk of the heart failing, or the risk of dying.

ABSTRACT

The electrocardiogram (ECG) is a common diagnostic tool in cardiology thanks to its high accessibility and low cost. However, in several cardiovascular diagnoses, including left ventricular hypertrophy (LVH), current conventional ECG measures and criteria have a poor diagnostic performance. LVH is associated with hypertension and diabetes, but is often missed by the standard 12-lead ECG. LVH is typically diagnosed by non-invasive imaging methods. Cardiovascular magnetic resonance (CMR) is the gold standard for diagnosing LVH. Advanced-ECG (A-ECG) is a term used to describe a combination of advanced ECG analysis methods, and has been shown to be of diagnostic and prognostic utility. The aims of this thesis were to investigate the ability of A-ECG to diagnose LVH, using CMR as reference, as well as investigating the prognostic ability of A-ECG measures with regards to morbidity and mortality.

We found that increased extracellular volume fraction by CMR reduces voltage measures of conventional ECG criteria for LVH, including the Sokolow-Lyon index and Cornell indices. This may explain the limited sensitivity of the ECG in detecting LVH. We further investigated different patterns of LVH based on the relation between increased mass and wall thickness, and found that the different patterns differ on their electrocardiographic manifestation by A-ECG. Furthermore, A-ECG had a higher diagnostic performance compared to conventional ECG LVH criteria.

The ECG detects electrical changes, while LVH represents a structural change. Therefore, the electrical changes associated with LVH may be better referred to as left ventricular electrical remodeling (LVER). LVER, defined as the A-ECG measure spatial QRS-T angle exceeding the upper limit of normal, was found to have a higher accuracy in diagnosing LVH compared to conventional ECG LVH criteria. We also found that patients with LVER have a worse prognosis compared to patients without LVER. Lastly, we optimized a score based on ECG and CMR measures, respectively, to predict morbidity and mortality, and found that ECG and CMR are both strong and independent predictors of events.

In conclusion, conventional ECG criteria lack sensitivity in detecting LVH, which may be explained by increased extracellular volume fraction or different structural patterns in LVH. A-ECG has a higher diagnostic accuracy than conventional ECG criteria for LVH and is prognostic beyond CMR measures. Lastly, we suggest that LVER should be used when electrical changes in LVH are addressed.

LIST OF SCIENTIFIC PAPERS

I. **Maanja M**, Wieslander B, Schlegel TT, Bacharova L, Abu Daya H, Fridman Y, Wong TC, Schelbert EB, Ugander M. Diffuse Myocardial Fibrosis Reduces Electrocardiographic Voltage Measures for Left Ventricular Hypertrophy Independent of Left Ventricular Mass. *J Am Heart Assoc*. 2017 Jan 22;6(1).

II. **Maanja M**, Schlegel TT, Kozor R, Lundin M, Wieslander B, Wong TC, Schelbert EB, Ugander M. The electrical determinants of increased wall thickness and mass in left ventricular hypertrophy. *J Electrocardiol.* 2019 Nov 13;58:80-86.

III. **Maanja M**, Schlegel TT, Kozor R, Bacharova L, Wong TC, Schelbert EB, Ugander M. Left ventricular electrical remodeling defined as an abnormal spatial QRS-T angle for electrocardiographic diagnosis and prognosis in left ventricular hypertrophy. *Submitted*.

IV. **Maanja M**, Schlegel TT, Fröjdh F, Niklasson L, Wieslander B, Bacharova L, Schelbert EB, Ugander M. An electrocardiography score predicts heart failure hospitalization or death beyond that of cardiovascular magnetic resonance imaging. *Submitted*.

CONTENTS

LIST OF ABBREVIATIONS

A-ECG	Advanced electrocardiography
AUC	Area under the curve
BMI	Body mass index
BPM	Beats per minute
BSA	Body surface area
CI	Confidence interval
CMR	Cardiovascular magnetic resonance
CT	Computed tomography
ECG	Electrocardiogram
ECV	Extracellular volume fraction
Gd	Gadolinium
GLS	Global longitudinal strain
GT	Global wall thickness
GTI	Global wall thickness index
HF	Heart failure
HR	Hazard ratio
ICM	Ischemic cardiomyopathy
IQR	Interquartile range
LGE	Late gadolinium enhancement
LV	Left ventricle
LVEDV	Left ventricular end diastolic volume
LVEF	Left ventricular ejection fraction
LVER	Left ventricular electrical remodeling
LVH	Left ventricular hypertrophy
LVM	Left ventricular mass
LVMI	Left ventricular mass index
MI	Myocardial infarction
MOLLI	Modified Look-Locker inversion recovery
MRI	Magnetic resonance imaging

NASA	National Aeronautics and Space Administration
NICM	Non-ischemic cardiomyopathy
NPV	Negative predictive value
NYHA	New York Heart Association
PPV	Positive predictive value
PSIR	Phase sensitive inversion recovery
ROC	Receiver operating characteristic
SD	Standard deviation
SSFP	Steady state free precession
SVD	Singular value decomposition
T	Tesla
UPMC	University of Pittsburgh Medical Center
VCG	Vectorcardiogram

1 RATIONALE

The focus of this thesis is electrocardiographic (ECG) diagnosis of electrical changes in structural changes of the heart including left ventricular hypertrophy (LVH) as measured by cardiovascular magnetic resonance (CMR) imaging. The ECG records the electrical conduction of the heart, and in a healthy person the ECG recording follows a specific pattern, but the pattern can be altered in cardiovascular disease.

Cardiovascular disease is as a major cause of morbidity and mortality in the world (1), and the ECG is one of the most commonly used diagnostic tools in cardiology owing to its accessibility and low cost. However, the ECG has a limited sensitivity and variable specificity in detecting disease (2). Advanced ECG (A-ECG) is a term used to describe a combination of advanced ECG analysis methods using digital signal processing, and statistically determined diagnostic scores based on large samples of imaging-verified health and disease. A-ECG parameters include derived vectorcardiographic (VCG) measures (3), QRS-wave and T-wave complexity measures obtained using singular value decomposition (4), heart rate and QT variability, high frequency components of the QRS, and other published methodologies. A-ECG has been shown to be more sensitive, as well as more specific, at identifying a number of cardiac diseases compared to conventional ECG (4). Thus, there are compelling reasons to reassess the role of the ECG in detecting cardiac electrical remodeling and related abnormalities. Recent developments in state-of-the-art CMR have made it possible to accurately perform quantitative characterization of myocardial tissue properties such as myocardial scarring, diffuse myocardial fibrosis, edema, ventricular mass and function, and quantitative perfusion at rest and during pharmacological stress. These recent developments make CMR an excellent non-invasive reference standard for understanding and improving the diagnostic accuracy of A-ECG.

2 INTRODUCTION

2.1 CARDIOVASCULAR DISEASE

Cardiovascular disease is a term that includes diseases of the heart, peripheral vessels, and brain. It is the leading cause of morbidity and mortality in the world (1, 5), and is a hindrance for sustainable human development (6). Cardiovascular disease typically affects people in the middle of their lives, and the costs comprise an increasing burden on society (6). Major risk factors for cardiovascular disease are hypertension, obesity, diabetes mellitus, high blood cholesterol, smoking, and physical inactivity (7-10).

2.1.1 Heart failure

In a healthy person, the heart pumps enough blood to meet the oxygen and metabolic demand of the body. Heart failure (HF) is a condition in where there is an inability of the heart to provide adequate blood supply in relation to demand, while preserving normal filling pressure. HF is a common disease worldwide, with an increased incidence and prevalence in the aging population. In developed countries, HF has an overall prevalence of 2%, and is more common with increasing age and reaches a prevalence of 10% at 85 years of age (11). The prevalence of HF is thus expected to increase in countries with an aging population (12). The mortality in HF is high, but can be reduced with correct diagnosis, management and treatment. HF often progresses slowly as a chronic condition but can also be acute. The diagnosis of HF can be demanding as many patients may have other diseases that mimic or disguise HF. Symptoms of HF are related to the lack of adequate oxygen supply and/or the retention of fluids due to the impaired cardiac function. Clinical hallmark signs include shortness of breath, crackles upon lung auscultation, and swelling of the legs, neck veins and/or abdomen. Besides clinical signs, laboratory tests and imaging can help the clinician diagnose HF or its many causes. The most utilized laboratory test is the blood level of brain natriuretic peptide (BNP) which increases as a result of an increased stretching in cardiac muscle tissue, due to *e.g.* volume overload (13). A wide range of imaging and functional tests are used including ECG, echocardiography, nuclear imaging, computed tomography, and CMR, with or without pharmacological or exercise stress, and invasive cardiac catheterization.

Heart failure has many causes, all of which impair the ability of the heart to efficiently pump blood, and can broadly be divided into ischemic, valvular, hypertensive, cardiomyopathic,

other, and unknown causes (14). Depending on symptoms, and level of physical activity, the New York Heart Association (NYHA) functional classification is typically used to define five stages of HF (15). According to the European Society of Cardiology Heart Failure Guidelines 2016 HF can also be divided into HF with preserved left ventricular ejection fraction (LVEF) of ≥50%, HF with mid-range LVEF of 40–49%, or HF with reduced LVEF of <40% (16).

2.1.2 Left ventricular hypertrophy

Left ventricular hypertrophy (LVH) is a cardiac condition defined as an increased left ventricular (LV) mass (LVM) (2). Hypertrophy refers to an increase in the volume of a cell, leading to enlarged tissues or organs. Hypertrophy is distinguished from hyperplasia in which the cells increase in amount, also leading to enlarged tissues or organs. Besides enlarged cardiomyocytes, the hypertrophic myocardium also undergoes complex interstitial changes such as an accumulation of focal or diffuse myocardial fibrosis, inflammation, fatty infiltration, edema, or ischemic changes (2). The increased LV mass can lead to an imbalance in the myocardial blood supply, and an abnormal reorganization of myocardial composition (17). This can cause HF due to mechanical, vasomotor, and electrical dysfunction (18-21). LVH is associated with an increased incidence of cardiovascular disease including HF, stroke, and coronary heart disease (22), all leading contributors to decreased quality-of-life, hospitalization, and death in developed countries (23). LVH is typically diagnosed by cardiac imaging including echocardiography and CMR, or by ECG. Importantly, echocardiographic findings of LVH, and LVH by ECG correlate poorly, but both provide independent prediction of mortality and morbidity (24). This suggests that the ECG provides information about LVH beyond the increase in LV mass *per se*.

LVH is defined as an increased LVM, but depending on the relation between mass and LV end diastolic volume (LVEDV), LVH can be subdivided into three different patterns (25): 1) concentric remodeling, defined as a normal LV mass with an increased wall thickness; 2) eccentric hypertrophy, defined as an increased LV mass with a normal wall thickness; and 3) concentric hypertrophy, defined as an increase in LV mass with an increased wall thickness. Global wall thickness (GT) has together with LVM been shown to accurately classify LVH into the different subtypes, illustrated in Figures 2.1 and 2.2, and is useful to predict prognosis (26).

Figure 2.1. Classification of LVH based on left ventricular mass and wall thickness

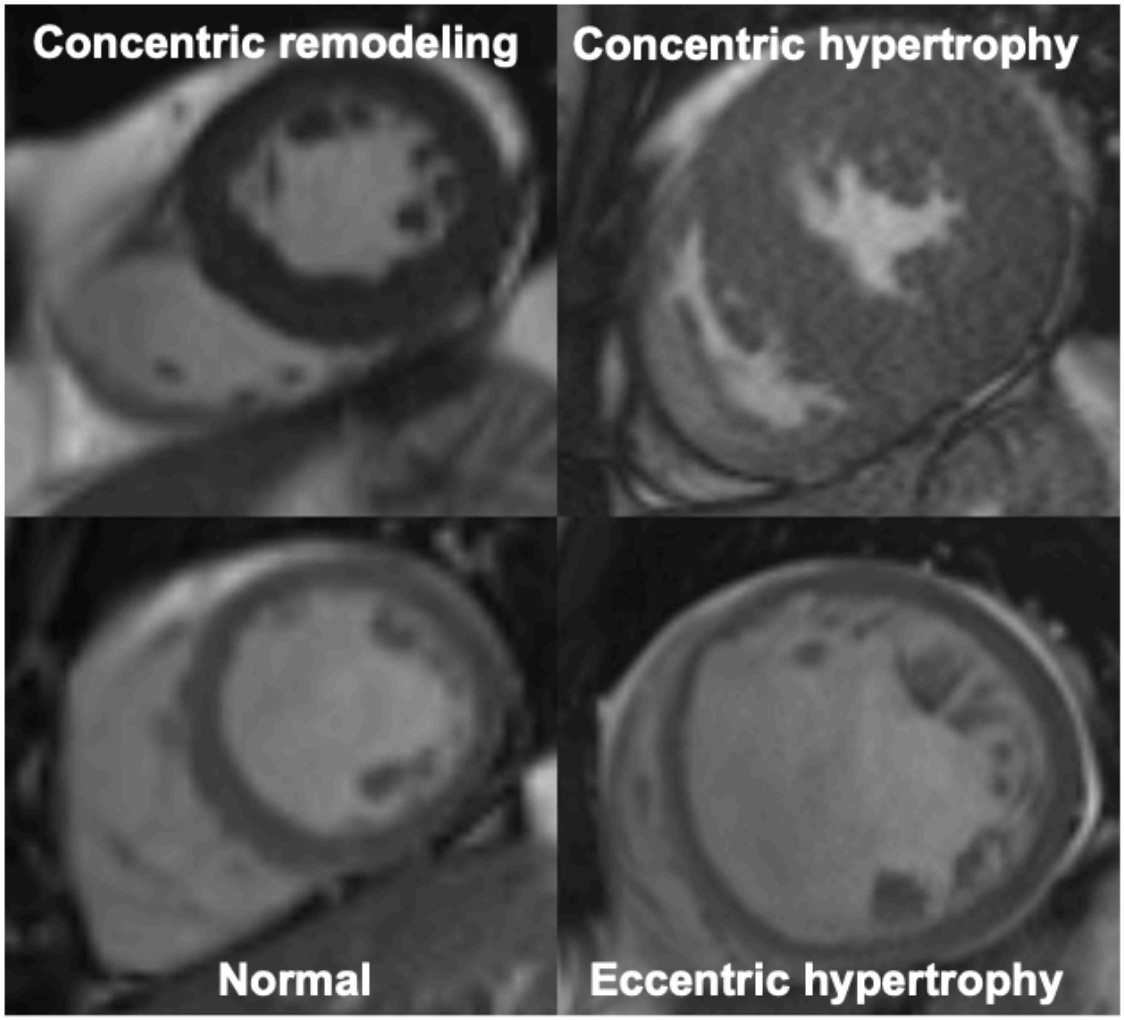

Figure 2.1: *Cardiovascular magnetic resonance images of four different hearts in a short-axis view. The four examples illustrate how normal and increased left ventricular mass index (LVMI) and left ventricular global wall thickness index (GTI) can classify left ventricular hypertrophy into three patterns: concentric remodeling, i.e. a normal LVMI and increased GTI (top left), eccentric hypertrophy i.e. an increased LVMI and normal GTI (bottom right), and concentric hypertrophy i.e. both an increase in LVMI and GTI (top right). Cut-offs for normal and increased (not explicitly shown) are the sex-specific 95% upper limit of normal in healthy volunteers (26). Figure adapted from Lundin, et al (27).*

Figure 2.2. Classification of LVH based on left ventricular mass and wall thickness

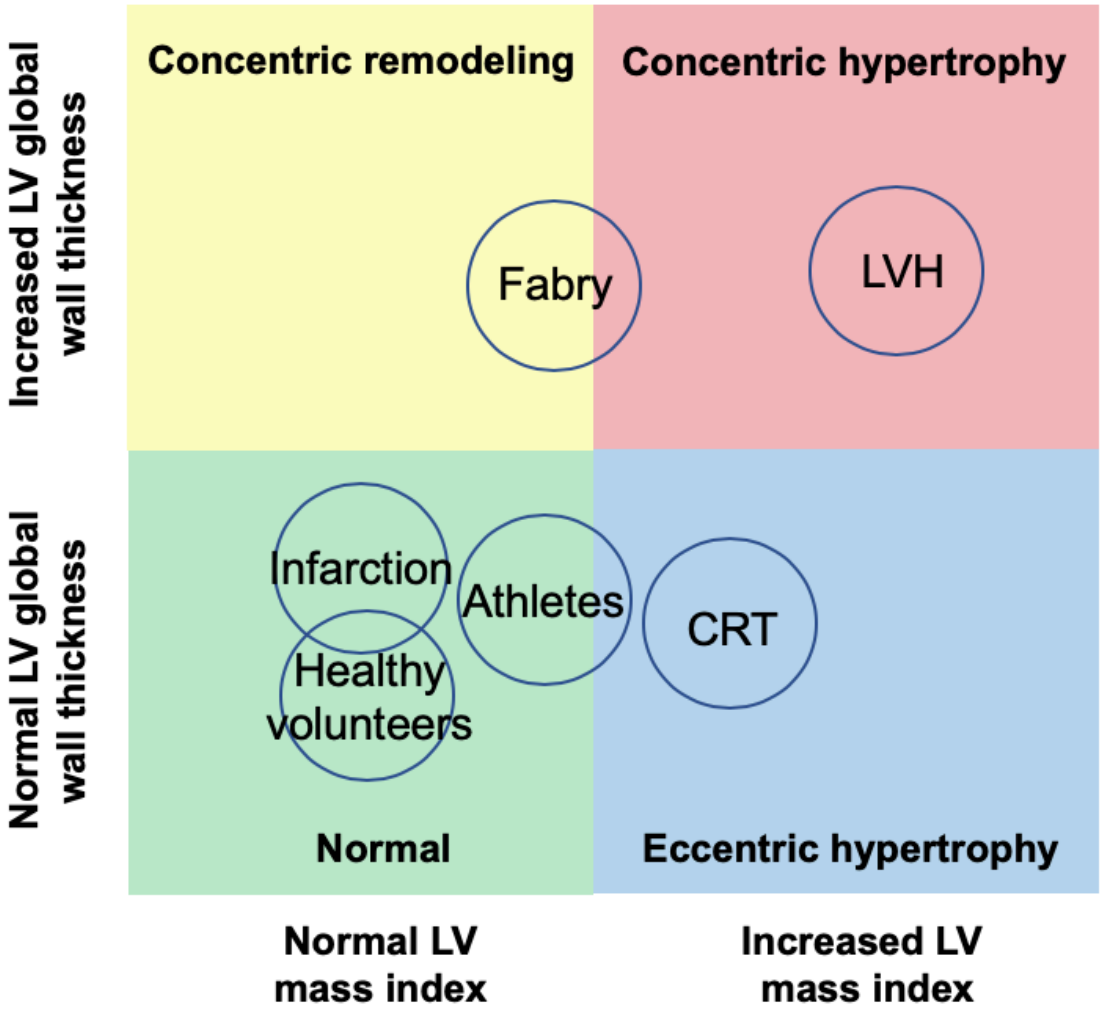

Figure 2.2: *A schematic figure of how normal and increased left ventricular (LV) mass index and LV global wall thickness index can classify left ventricular hypertrophy into three patterns: concentric remodeling, eccentric hypertrophy, and concentric hypertrophy. Cut-offs for normal and increased (not explicitly shown) are the sex-specific 95% upper limit of normal in healthy volunteers (26). The blue circles illustrate roughly how different patient groups are classified according to the schematic figure. The following patient groups are included: healthy volunteers, patients with recent acute ST-elevation myocardial infarction (Infarction), endurance athletes (Athletes), cardiac resynchronization therapy (CRT) candidates, patients with the genetic disorder Fabry disease (Fabry), and patients with at least moderate left ventricular hypertrophy (LVH). Figure adapted from Lundin, et al (27).*

2.1.3 Left ventricular hypertrophy and diffuse myocardial fibrosis

Fibrosis is a global health problem and present in nearly all forms of cardiovascular disease (28). It is a common final end point and is associated with impaired LV function, symptoms, and adverse prognosis. It has previously only been quantified by biopsy and histology, and as a result, it is not fully understood. CMR studies show that hypertrophic myocardium may include diffuse myocardial fibrosis and/or focal myocardial fibrosis (29). Diffuse myocardial fibrosis is a global abnormal accumulation of extracellular matrix in the myocardium (17), whereas focal fibrosis, also known as scar, is focal and can be a result of myocardial infarction (MI) or other non-ischemic injuries such as myocarditis (30). The presence of these may influence the ECG interpretation of LVH (29). In the absence of amyloidosis, a disease characterized by an abnormal accumulation of proteins in tissue, or in the absence of myocardial edema, the primary interstitial component leading to an expansion in the extracellular matrix is myocardial collagen (18).

In response to stress or injury, cardiac fibroblasts proliferate and differentiate into myofibroblasts. These cells secrete fibronectin, collagen I, and collagen III, which form extracellular matrix and fibrosis (29). Myofibroblasts also express pro-fibrotic and pro-inflammatory factors that contribute to fibroblast proliferation and inflammation (28). This can lead to HF (17) due to mechanical, electrical or vasomotor dysfunction (29). An increase in myocardial fibrosis is a part of normal ageing (29), however, it progresses faster in diseases such as hypertension, diabetes mellitus, aortic stenosis, and hypertrophic cardiomyopathy. Furthermore, myocardial fibrosis is an independent contributor to mortality and morbidity, and the amount of fibrosis is directly correlated with arrhythmias and sudden cardiac arrest (29), as well as to hospitalization for heart failure and death (31). In comparison to focal fibrosis, diffuse myocardial fibrosis may be reversible and is a target of pharmacotherapy, *e.g.* targeting the renin-angiotensin-aldosterone system as it has an impact on the excessive accumulation of collagen I and III in myocardial extracellular matrix (32), or a target of immunotherapy (33).

Figure 2.3. Histological analysis of myocardial tissue

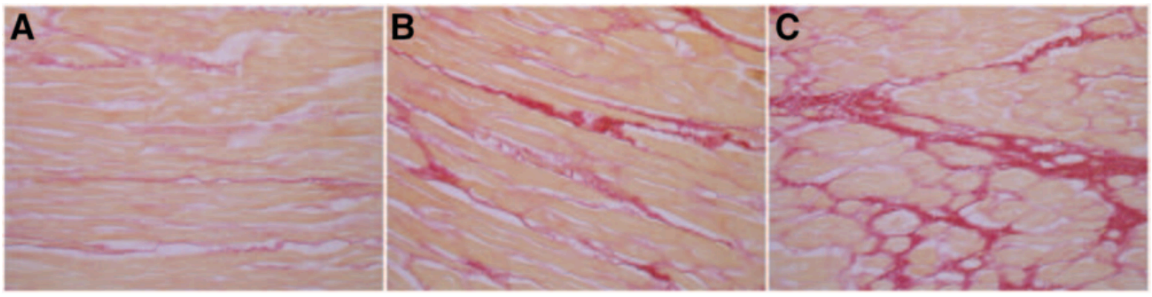

Figure 2.3: *The myocardial tissue samples A, B, and C were embedded in paraffin. Picrosirius red was used to stain collagen (fibrosis) red/pink, and to stain myocytes yellow. The samples demonstrate a A) 8%, B) 16%, and C) 36% collagen volume fraction, forming the extracellular volume. Figure reproduced from Miller, et al (34), with permission.*

2.2 ELECTRICAL CONDUCTION SYSTEM OF THE HEART

Like many other cells in the body, cardiomyocytes can generate electrical potential. This occurs by a coordinated opening of voltage-gated channels with a selective permeability for sodium ion (Na^+), potassium ion (K^+), and calcium ion (Ca^{2+}) channels, respectively. These are located in the lipid bilayer cell membrane, leading to a rapid change in voltage across the membrane. At rest, the concentration of potassium is relatively high inside the cell, and the sodium concentration is high outside of the cell. The normal resting membrane potential of a cardiomyocyte is -90 mV, which approximately corresponds to the equilibrium of K^+. The action potential starts with a rapid inflowing current of Na^+ and Ca^{2+} ions, whereby the cell depolarizes and the membrane potential increases and becomes positive (35). The action potential triggers different intracellular processes including contraction of the cell. The cardiomyocytes are connected through gap junctions (36), which are essentially non-selective channels through which the ions can flow cell-to-cell downstream, and a wave-like spread of action potentials is generated, leading to a synchronous contraction of the cardiomyocytes. After the depolarization, the intracellular K^+ ions flow out of the cell leading to repolarization, and the cell returns to its negative resting membrane potential (35). Gap junctions are important for the rapid spread of the action potential. When the action potential has terminated, sodium-calcium and sodium-potassium pumps located in the cell membrane restore the concentration of ions, and a new action protentional can start over.

Figure 2.4. Myocardial action potential and the ECG

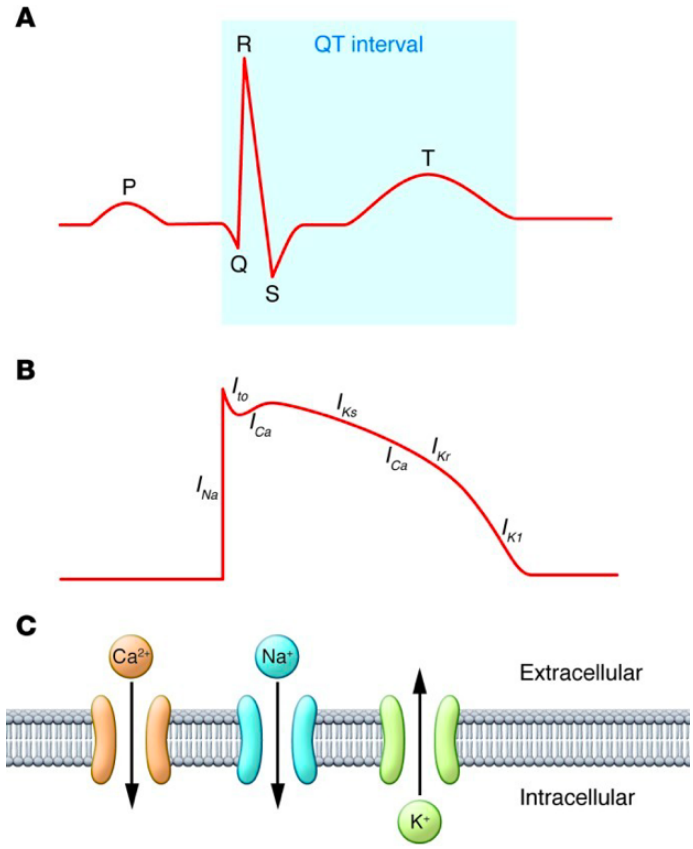

Figure 2.4: *The temporal relation between the A) surface ECG, where the P-wave indicates the atrial depolarization, the QRS-wave the ventricular depolarization, and the T-wave the ventricular repolarization, B) the cardiomyocyte action potential with the depolarization and repolarization phases, and C) the inward depolarizing currents of Na^{+} and Ca^{2+}, and the outward repolarizing currents of K^{+}. Figure reproduced from George (37), with permission.*

Pacemaker cells are specialized cardiomyocytes with an ability to spontaneously initiate an action potential (38), and they form the electrical conduction system of the heart. In a healthy heart, pacemaker cells in the sino-atrial (SA) node, located in the roof of the right atrium (39) as shown in Figure 2.5, start each heartbeat. An electrical signal impulse begins to depolarize the atrial myocardial cells which leads to the atrial contraction. The electrical impulse then reaches the atrioventricular (AV) node, located in the right atrial floor, where the signal is delayed. After this, the electrical signal passes His' bundle, through the ventricular septum, and into the left and right bundle branches. The right bundle branch divides into a delicate network called Purkinje fibers in the right ventricle that depolarize myocytes. The left bundle branch divides into an anterior and a posterior fascicle which subsequently divide into fine Purkinje fibers, and depolarize the ventricular myocardial cells.

Figure 2.5. Electrical conduction system of the heart

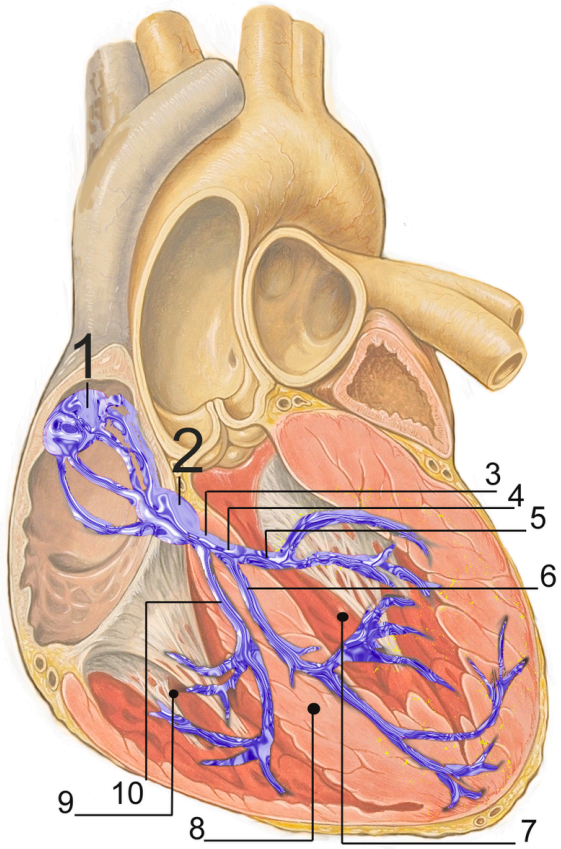

Figure 2.5: *The main components of the electrical conduction system of the heart: 1) sinoatrial node, 2) atrioventricular node, 3) bundle of His, 4) left bundle branch, 5) left-posterior fascicle, 6) left-anterior fascicle, 7) left ventricle, 8) ventricular septum, 9) right bundle branch, and 10) right ventricle. Figure reproduced under a creative commons license. Original heart by illustrator Patrick Lynch and cardiologist Carl Jaffe, and electrical conduction system by J. Heuser.*

In cardiovascular disease, the electrical propagation and the heart rhythm may vary, which can be diagnosed by ECG. The electrical changes do not necessarily follow anatomical or structural changes of the heart (40), but are part of a complex process referred to as electrical remodeling (41). Previous studies show that changes in cardiac action potential are critical in the early process in the chain of events leading to the development of myocardial hypertrophy and heart failure (42-44).

2.3 ELECTROCARDIOLOGY

2.3.1 Electrocardiography

As cardiology became a distinct medical specialty, various diagnostic techniques emerged and developed. The first human electrocardiographic recording was introduced more than a century ago by Augustus Waller in 1887 (45). However, the first clinically useful electrocardiogram was recorded by Willem Einthoven following his invention of the string galvanometer in 1901. The ECG signal was obtained from a patient by placing two extremities in saline solution, which led the electrical impulses from the heart to the electrocardiograph.

In modern times, the ECG signal is obtained through skin electrodes placed on the body that capture the electrical activity of the depolarization and repolarization of the heart. The signal in the conventional 12-lead ECG is derived from ten electrodes places on the skin; one electrode on each limb including a ground (limb leads), and six electrodes on the torso (precordial or chest leads). The six precordial leads, called V1-V6, are placed at the level of the heart as standardized in 1938. The limb leads are placed on the right arm, left arm, and left foot, according to the convention proposed by Einthoven, creating the three limb leads (46). An additional limb electrode placed on the right foot serves as a ground. Einthoven assigned the letter P, Q, R, S, and T to the deflections of the ECG waveform. Initially, the waveforms were named the letters A, B, C, and D, but after major adaptions of the ECG, the letters were changed to the second half of the alphabet to denote an updated ECG system (47). He also described ECG features of various cardiovascular disorders. In 1924, Einthoven was awarded the Nobel Prize in Medicine for his work (48). Since then, the electrocardiograph has gone through different advancements, and can now have the size of a watch or smaller, and the ECG can be sent wirelessly to a computer for digital analysis.

History of Advanced ECG

A-ECG is a combination of more advanced ECG techniques based on a digital 10-second ECG recording, or longer (5 minutes), and often sampled at a higher frequency than the conventional ECG. The A-ECG techniques include conventional ECG parameters, vectorcardiography, QRS complex and T wave complexity, high frequency QRS wave and late potentials, P wave analysis, and beat-to-beat RR- and QT-variability A-ECG is also known as Space-EKG as the A-ECG software was developed at the National Aeronautics and Space Administration

(NASA) Johnson Space Center, Texas, USA, to better detect and prevent cardiovascular disease in astronauts.

Figure 2.6. ECG lead placement and ECG waves

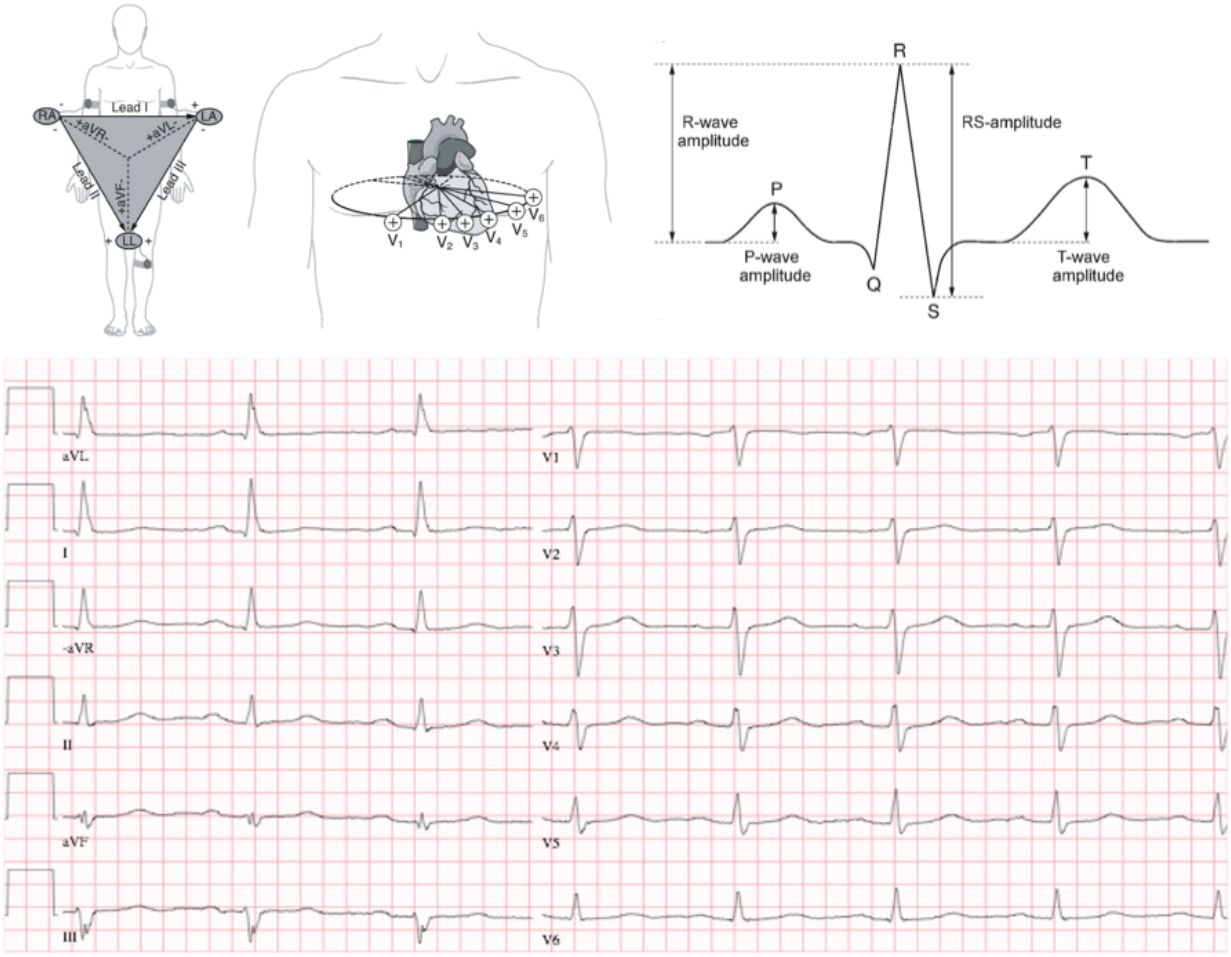

Figure 2.6: ***Upper panel****. The standard ECG leads constitute of six extremity leads and six precordial leads. The extremity leads (aVL, I, -aVR, II, aVF, III) are placed on the limbs and record the voltage difference in the frontal plane. The precordial leads (V1-V6) are placed on the chest wall and record the voltage difference in the horizontal plane. The P wave and QRS complex display the atrial and ventricular depolarization, respectively, and the T wave displays the ventricular repolarization. Along the vertical direction of the ECG leads, wave amplitudes are measured, and along the horizontal direction heart rate and wave durations are measured. Figure adapted from Koelsch, et al (49), with permission.* ***Lower panel.*** *A normal conventional 12-lead ECG with limb and precordial leads. The limb leads are displayed in the order of the Cabrera sequence (aVL, I, -aVR, II, aVF, III), as originally presented by Fumagalli (50). The Cabrera sequence is commonly used in Europe including in Sweden.*

2.3.2 Vectorcardiography

In 1920, Hubert Mann described the "monogram" (51), which later on was called the vectorcardiogram (VCG). While a standard 12-lead ECG references the sum of the electrical-potential vectors from de- and repolarized cardiomyocytes to a scalar, one-dimensional plane, the VCG displays the vectors as a loop in the three-dimensional space. Three perpendicular two-dimensional planes; the frontal, horizontal, and (left) sagittal plane, illustrate the three-dimensional spatial direction and magnitude of the vectors of the heart's electrical activity (52). The VCG is useful due to its visual representation of the electrical activity and its spatial variation during the cardiac cycle (53). Initially, the VCG was constructed from a 3-lead ECG with the electrodes placed in the frontal plane of the torso in a modified Einthoven triangle. A VCG can also be derived from a standard 12-lead ECG using the Kors' transform, a mathematical matrix validated using simultaneously recorded 12-lead ECGs and VCGs (3, 54), or using the inverse Dower matrix (55). For a number of reasons likely related to a combination of technical, interpretation-related, and acquisition standardization-related complexities, the VCG was effectively abandoned as a widely used clinical tool in the latter half of the twentieth century (56). However, recent developments, and computational resources in modern electrocardiographs, make it easier to obtain, display and interpret derived VCGs today.

The VCG shows the magnitude and angular direction of the electrical activity at each time frame in the cardiac cycle. The QRS-T angle is an established VCG measure defined as the angle in three-dimensional space between the peak magnitude of the QRS and T loop vectors, respectively. It has historically been measured by VCG using dedicated lead placement, but can now be derived from a standard 12-lead ECG. Similarly to the concordance or discordance of the QRS wave and T wave in a given lead in the conventional ECG, the QRS-T angle reflects the dispersion between the ventricular depolarization and repolarization (57). In a healthy heart, the angle is small, but it increases as a result of myocardial disease process (58) including in LVH (*Study III*), hypertension (59), diabetes (60), and hemophilia A (61). The QRS-T angle is also an independent predictor of cardiovascular mortality (62).

Figure 2.7. Vectorcardiogram and the QRS-T angle

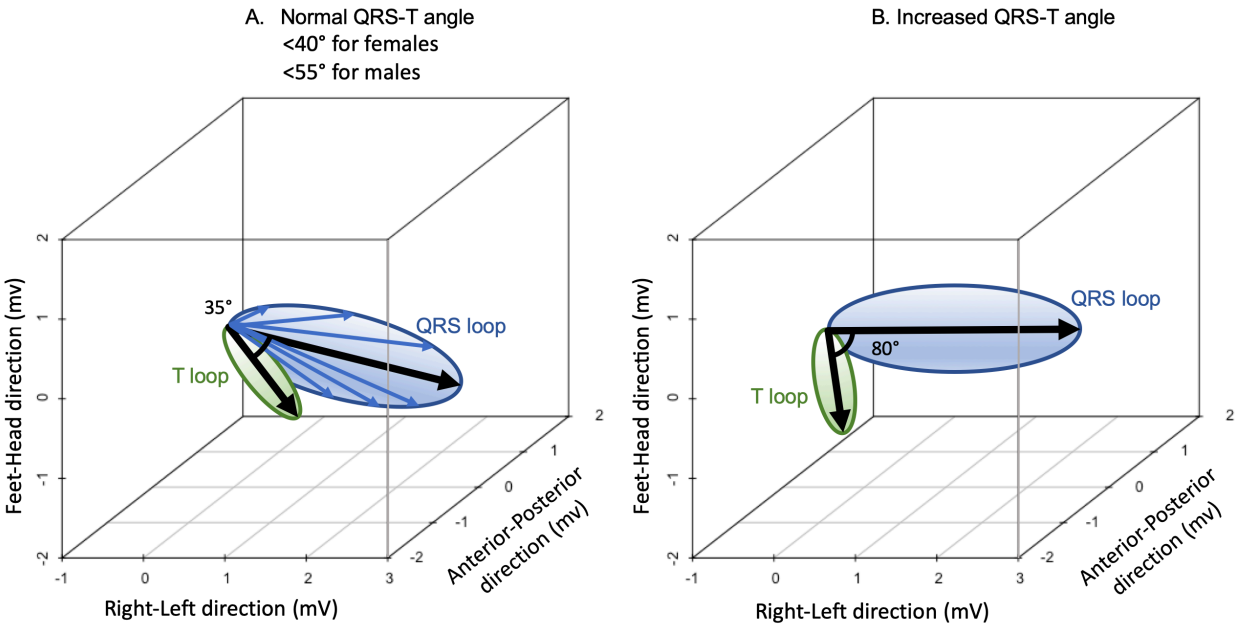

Figure 2.7: *The vectorcardiogram (VCG) is useful as it visualizes the cardiac action potential in the three-dimensional space. The blue arrows show the ventricular net depolarization vectors' magnitude and direction for each time frame. When the tips of the vectors are connected by the blue line, they form what is called the QRS loop. The same is applied for the T loop, but it represents the repolarization of the ventricle.* ***A.*** *A schematic illustration of the VCG measure spatial QRS-T angle, which is the angle between the largest vector in the QRS loop and T loop, respectively.* ***B.*** *An increased spatial QRS-T angle, which can be encountered in e.g. left ventricular hypertrophy. Figure modified from Study III.*

Besides three-dimensional VCG measures, polarcardiographic measures can also be derived from the 12-lead ECG. In addition to the VCG, which plots the direction and the magnitude of the heart's electrical vector, the polarcardiogram also plots it over time, and in a spherical/polar coordinate system (63). The polar vector, which is illustrated in a polarcardiogram, has previously been shown to deviate in the setting of LVH in comparison to healthy subjects (64).

2.3.3 QRS wave and T wave complexity

Detailed studies of ECG waveforms can be obtained through singular value decomposition (SVD) performed on a conventional 12-lead ECG. SVD is a mathematical signal processing technique, whereby the depolarizing QRS-waves and repolarizing T-waves can be spatially

characterized in terms of orthogonal bases. The orthogonal bases, also referred to as eigenvectors or eigenvalues, are the vectors that span a room in a certain dimension, as illustrated in Figure 2.8. The magnitude of the eigenvectors represents the "energy" present in the respective wave. The eigenvectors are typically measured in microvolts, and two or more eigenvectors can be combined with each other to create sums and/or ratios of eigenvectors.

Figure 2.8. Eigenvectors

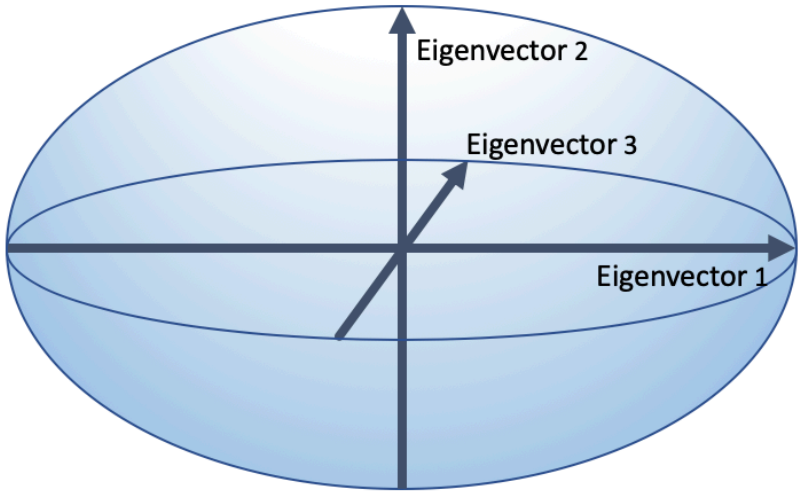

Figure 2.8: *Eigenvectors illustrated in the three-dimensional space of an ellipse. The first base, or eigenvector, is the largest vector in the ellipse, Eigenvector 1. The second eigenvector is the second largest vector in the ellipse, Eigenvector 2, and is orthogonal to Eigenvector 1. The third eigenvector is the third largest vector, Eigenvector 3, and is orthogonal to Eigenvector 1 and Eigenvector 2, respectively. Together the three eigenvectors span the room of the three-dimensional ellipse.*

The standard 12-lead ECG is constructed from ten electrodes and eight unique channels: lead I, lead II, and lead V1 – V6. The remaining extremity leads can be derived from lead I and lead II. The eight unique channels represent eight dimensions of the electrical propagation. Thus, eight different eigenvectors for the (eight-dimensional) P loop, QRS loop and T loop, respectively, can be calculated.

In a healthy heart, the first eigenvector in a de- or repolarization loop accounts for most of the energy that is present (65). In a homogeneous de- and repolarization there is also a presence of substantial energy in the second and third eigenvectors, and the energy decreases drastically as the eigenvectors increase. In cardiac disease, the energy may shift and become substantial even

in higher eigenvectors. Quantification of the magnitude of the respective eigenvectors has been shown to be diagnostically useful in cardiovascular disease (4, 66, 67).

2.3.4 Left ventricular hypertrophy by electrocardiography

ECG criteria for LVH were originally established from autopsies of enlarged ventricles or clinical features of the patients (68). Later, new imaging modalities, such as 2- and 3-dimensional echocardiography and CMR, were adopted as the reference standard for determining the presence and severity of LVH. Such modalities became the reference standard for the ECG changes associated with LVH (68). LVH by ECG is typically assessed by various criteria. A total of 37 different criteria for LVH by ECG are recommended by the American Heart Association (2), but the Sokolow-Lyon voltage index, Romhilt-Estes criteria, and Cornell voltage and voltage product, respectively, are commonly used. In 1940 Sokolow and Lyon introduced a set of ECG criteria based on the sum of the R wave in lead V5 (R_{V5}) or R_{V6} and S_{v1} (sum >3.5 mV) (69). Today, the Sokolow-Lyon index is widely recognized clinically for diagnosing LVH. The Cornell voltage is the sum of R_{aVL} and S_{V3} voltage (sum >2.0 mV for women and >2.8 mV for men) (70). More recently, several criteria have been added, making the clinical ECG diagnosis of LVH more complex (68).

Figure 2.9. Electrocardiographic LVH

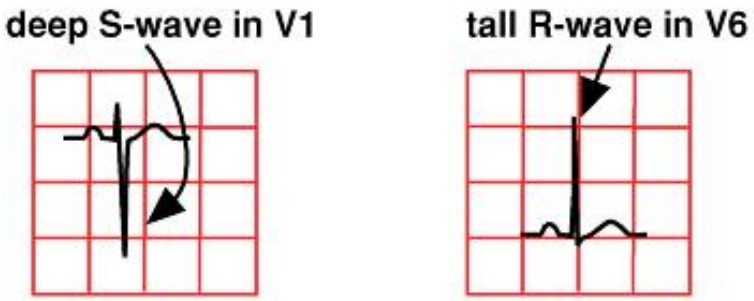

Figure 2.9: *High QRS-amplitudes on the ECG can be present in left ventricular hypertrophy. The combined amplitudes of the S-wave in lead V1, and the R-wave in lead V5 or V6, are increased in left ventricular hypertrophy, according to the Sokolow-Lyon voltage index.*

The diagnostic performance of the conventional ECG LVH criteria vary greatly, with a sensitivity typically around 50%, and a specificity typically approaching 90% (68). Because of this, a patient who is positive by one criterion is often negative by another criteria (68). A large

study identified patients (n=9194) with mild or severe hypertension, and either a positive Sokolow-Lyon index or Cornell voltage, were enrolled in a pre-enrollment screening (71). However, only 11.2% of the patients met both sets of criteria. In addition, different clinical characteristics and baseline demographics were associated with the two sets of criteria (71). Furthermore, varying sensitivity has also been reported in patients with different underlying cardiac disease (72). Regardless of the poor sensitivity and varying specificity of the conventional ECG criteria for detecting LVH, they may be used to predict all-cause mortality (73).

Conventional ECG LVH criteria typically have a low sensitivity and varying specificity in detecting LVH, defined as an increased LV mass (74). LVH criteria by ECG are typically based on increased QRS complex amplitudes and prolonged durations, deviations in the ST-T regions, and electrical axis deviations. However, these measures and criteria are not always proportional to increased LV mass (2). The ECG reflects the generated electric activity which does not exclusively depend on increased mass (75).

2.3.5 Left ventricular electrical remodeling

Electrocardiographic LVH by conventional criteria is a misleading term as the ECG detects electrical changes in the heart while LVH is an anatomical and structural change, and anatomical and electrical changes are two different phenomena. Furthermore, the ECG has repeatably been shown to lack diagnostic accuracy whereas cardiovascular imaging is more accurate. The classical conceptual ECG LVH model, that heart disease leads to chamber enlargement, which leads to increases in QRS amplitudes and durations, is greatly simplified (40). It is based on a theoretical model of "ideal" LV hypertrophy, *i.e.* that the hypertrophy is symmetrical and diffuse, and that the electrical activation is unchanged, and this is how clinical cases are conventionally explained (76). Computer simulations of electrical propagation in different types of hypertrophy show that, depending on the arrangement of the hypertrophic cardiomyocytes, the ECG model of "ideal" hypertrophy results in increased QRS vectors (77). However, the more accurate *in vivo* scenario is much more complex with structural, bioelectrical and biochemical changes that interact and lead to mechanical, electrocardiographic, and rhythm effects. Furthermore, the tissue surrounding the heart, and body fat varies greatly among individuals, and also affect the electrical recordings.

Electrical remodeling is a term that includes the complex active and passive electrical properties of the myocardium. Electrical and structural remodeling are continuous processes and start in the early stages of cardiac pathology, and it is likely that electrical changes are manifested on the ECG before arrhythmias (78). Furthermore, LVH and structural heart disease include microscopic structural changes, and changes in metabolism, gap junctions, ion channels, and in the gene expression, all of which are substrates for triggering and maintaining arrhythmias (79-82).

Figure 2.10. Classical and extended models of ECG diagnosis of LVH

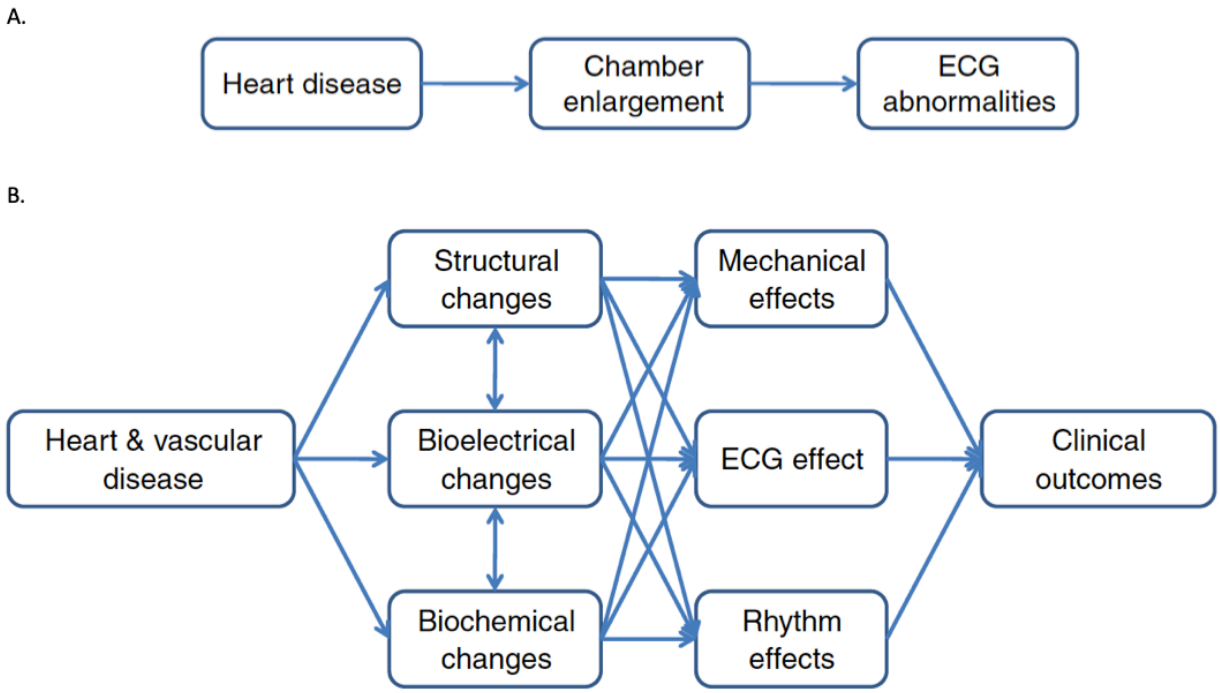

Figure 2.10: *Conceptual models of electrocardiographic diagnosis of left ventricular hypertrophy. A. The "classical" conceptual model that heart disease leads to chamber enlargement and subsequent ECG abnormalities. B. An extended conceptual model for ECG diagnosis of left ventricular hypertrophy, as proposed by the Journal of Electrocardiology LVH Working Group. Figure A and B reproduced from Bacharova, et al (40), with permission.*

The Journal of Electrocardiography LVH working group (40) has previously proposed that the term left ventricular electrical remodeling (LVER) should be used when describing the electrical changes associated with LVH. However, the definition and criteria for LVER were not proposed. Therefore, one of the main aims of *Study III* was to define ECG criteria for LVER.

2.4 CARDIOVASCULAR MAGNETIC RESONANCE IMAGING

Cardiovascular imaging can be accomplished using various techniques including CMR, echocardiography, single photon emission tomography (SPECT), positron emission tomography (PET), and x-ray computed tomography (CT). CMR was introduced as a clinical tool in the early 1980s, and through various developments and applications it is now the reference standard for evaluating cardiac function, structure (83), viability, and myocardial perfusion (84). It is used to assess myocardial ischemia, cardiomyopathies, myocardial interstitial disease, congenital heart disease, and myocardial inflammation, among other conditions. CMR is relatively expensive and less readily available compared to echocardiography, but when operated by experienced operators, CMR has a high diagnostic accuracy, and is associated with few risks. In comparison to CT and SPECT, CMR exams can be performed repeatedly without requiring exposure to ionizing radiation. Also, a gadolinium-based contrast agent is often administrated intravenously as a part of the CMR exam, and adverse reactions including anaphylaxis are exceedingly rare (<1 in 10,000 cases) (85).

Generating images using MRI scanners is a complex physical and technical procedure. Briefly, radio waves, strong magnetic fields, and magnetic field gradients are utilized to image the body and visualize different tissue properties (86). Clinical CMR is generally performed using 1.5 tesla (T) or 3.0 T magnets. The signal in the images is derived from hydrogen atoms, which are abundant in the human body. When a patient is inside the scanner and exposed to the strong magnetic field, the protons in the hydrogen nuclei align in the magnetic field. By exciting the nuclei with a radio frequency pulse, a signal is obtained through a resonance phenomenon (87). By varying the magnitude, spatial directions, and timing of the radio frequency pulses and the magnetic field gradients, the MRI scanner is capable of producing high-resolution images that reflect different properties of the tissue, such as proton density or relaxation properties, denoted by the time constants T1 and T2 (88).

2.4.1 Extracellular volume fraction

T1 measurement by CMR involves measurement of the time constant of relaxation, or the recovery, of the proton orientation in relation to its original position in the magnetic field after being excited by a radio frequency pulse. T1 maps by CMR provide quantitative myocardial tissue characterization with a high signal-to-noise ratio (23). T1 mapping before and after intravenous administration of a gadolinium-based contrast agent can be used to measure the

size of the myocardial extracellular space. The contrast agent is small enough to distribute freely in the extracellular space, but large enough that it does not enter living cells. The contrast agent shortens the relaxation time and thus lower T1 values (23). The inverse of T1 is referred to as R1, and the difference in R1 before and after admission of gadolinium contrast is referred to as ΔR1. The ratio between myocardial ΔR1 and blood ΔR1 is directly proportional to the ratio between myocardial ECV and blood ECV, *i.e.* the non-hematocrit fraction of whole-blood (89). With a known blood and myocardial ΔR1, and a venous hematocrit blood sample, myocardial ECV can be calculated (90). Importantly, myocardial ECV by CMR has been shown to closely reflect the histologically determined collagen volume fraction, which is the histological hallmark of diffuse myocardial fibrosis (30), and associates with worse clinical outcomes (31).

2.4.2 Late gadolinium enhancement

In myocardial infarction, myocardial cells are damaged due to prolonged ischemia leading to rupture of cell walls, cell necrosis, and a loss of cellular function (91). Ischemic cardiomyopathy (ICM) is characterized by focal fibrosis following myocardial infarction involving the subendocardium, the part of the myocardium most susceptible to ischemia. Depending on infarct size, the fibrosis may extend transmurally to the epicardium to a varying degree. CMR with late gadolinium enhancement (CMR-LGE) can detect areas of infarction as small as one gram of tissue (92). Non-ischemic cardiomyopathy (NICM) is a diverse set of pathologies involving the myocardium in the absence of significant coronary artery disease, and is characterized by a reduced left ventricular (LV) systolic function (93). NICM is associated with non-ischemic focal fibrosis patterns typically engaging the mid-wall, epicardium, or the global endocardium. Due to its high resolution and high contrast-to-noise ratio, CMR-LGE provides a clear differentiation between myocardial scar patterns in ICM and NICM (84).

Figure 2.11. Hyperenhancement patterns in ischemic and nonischemic disease

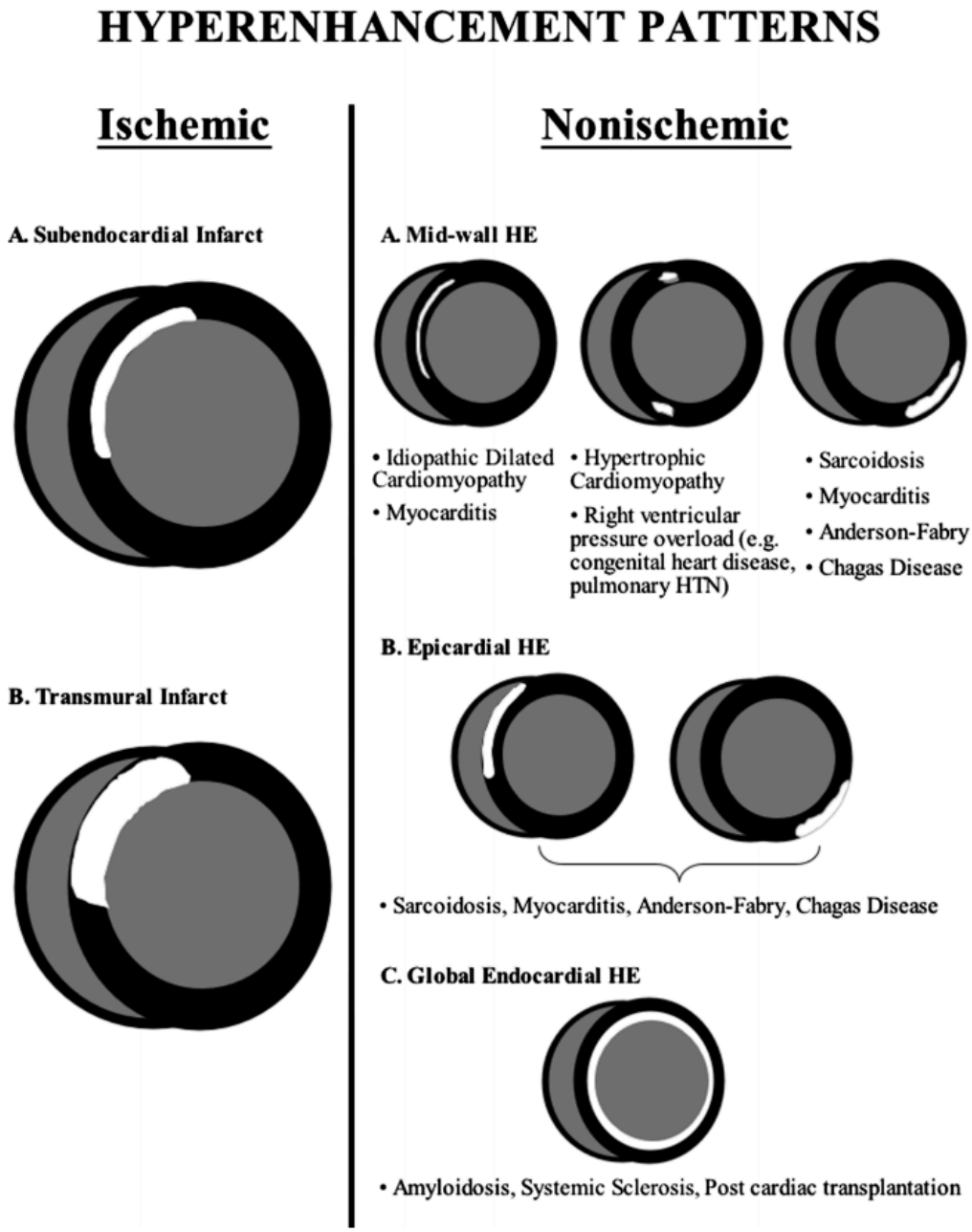

Figure 2.11: *Hyperenhancement patterns of ischemic and non-ischemic myocardium in cardiovascular magnetic resonance short axis slices. In ischemic disease, the endocardium is hyper enhanced, as the subendocardium is the part of the myocardium most susceptible to ischemia. In non-ischemic disease, isolated mid-wall, epicardial, or global endocardial, hyperenhancement patterns are present. HE indicates hyperenhancement. Figure reproduced from Mahrholdt, et al (94), with permission.*

2.4.3 Volume, mass, and function

Due to its excellent reproducibility and accuracy, CMR is the gold standard for assessing left ventricular volumes, mass, and systolic function (95). CMR uses cine imaging by repeatedly imaging the heart, one slice at a time, throughout the cardiac cycle. Below follows a list of CMR parameters commonly used in clinical evaluations, as well as within the scoop of this thesis. Several sex- and age-specific values of normality for these measures have been proposed. The studies in this thesis have used the reference values based on the work by Maceira, *et al* (96), unless otherwise specified.

- **Left ventricular ejection fraction (LVEF)** is the fraction, in percent, of blood in the left ventricle that is pumped out into the circulation system at every heart beat. Left ventricular ejection fraction (LVEF) is a widely-used marker for HF, but has well-known limitations in diagnosing HF (97). Nevertheless, LVEF is associted with adverse prognosis in the setting of HF (97, 98).
- **Global longitudinal strain (GLS)** reflects LV myocardial shortening, in percent, in the longitudinal direction, and is a measure of LV function. GLS shows prognostic value superior to LVEF (99), and new findings suggest GLS to be a better marker for impaired LV function than LVEF in patients with preserved LVEF (100). The heart also contracts in the circumferential direction, and that shortening in percent is referred to as global circumferential strain (GCS), and is also a marker for impaired LV function (100).
- **Left ventricular mass (LVM)** is the mass, in grams, of the myocardium. An increase in LVM is an independent risk factor for cardiovascular events (101). Due to the wide distribution on LVM in a normal population, it is often adjusted by indexing to body surface area (BSA, LVMI) (102).
- **Left ventricular end diastolic volume (LVEDV)** is the volume, in millilitres, of the left ventricle at the end of diastole – right before the onset of LV ejection, and thus when the LV volume is the largest. In a healthy heart, the volume is normal, but increases in certain pathologies, such as eccentric hypertrophy or dilated cardiomyopathy. Similar to LVM, EDV is often adjusted to BSA. The relationship between LVM and LVEDV can be used to estimate the left ventricle global wall thickness (GT), which is useful when characterizing different patterns of LVH (26).

Figure 2.12. Different CMR images

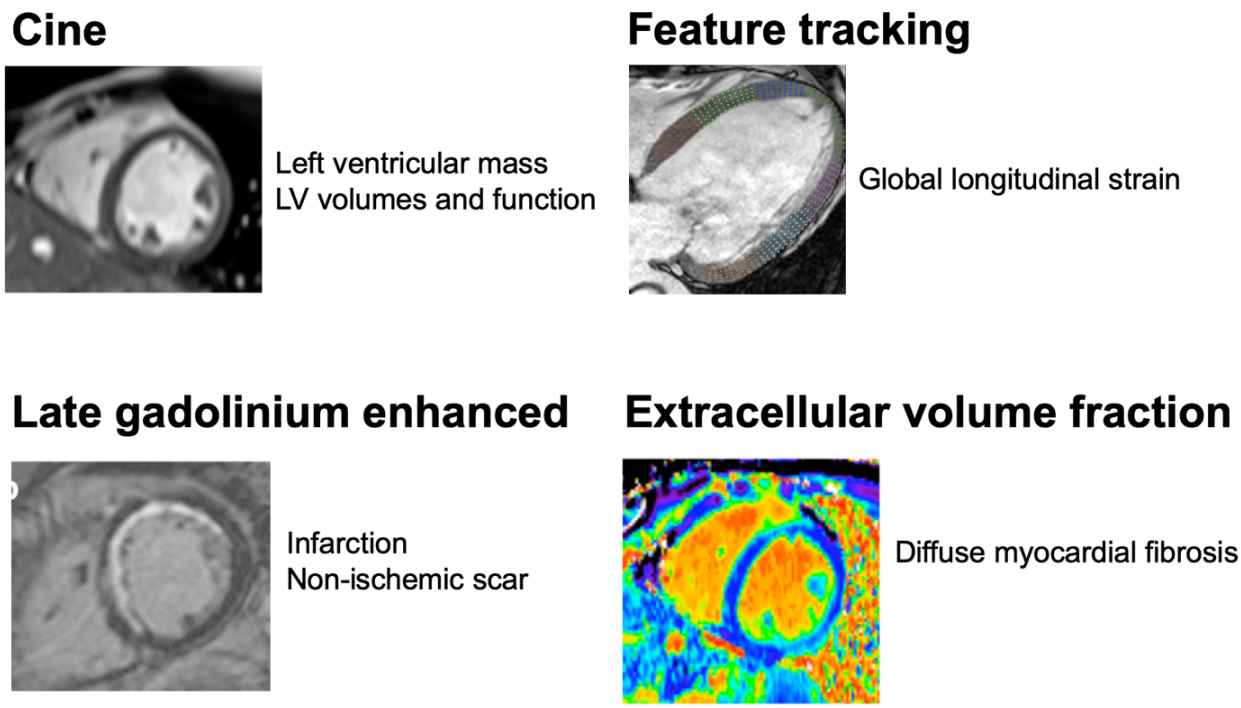

Figure 2.12: *Different CMR images from the top left: cine image(s), used to quantify left ventricular mass and assess left ventricular volumes and function; feature tracking, used to quantify global longitudinal strain, which is shortening, in percent, in the longitudinal direction; late gadolinium enhanced image, used to quantify myocardial infarction and non-ischemic scar size, and; extracellular volume fraction maps, which has been shown to correlate to diffuse myocardial fibrosis.*

2.5 PREDICTION MODELS

It has been shown that conventional ECG criteria lack sensitivity and specificity in detecting cardiac disease. In this thesis, we investigate if any – or if a combination of any – A-ECG parameters can improve the ability to diagnose LVH. A-ECG analysis encompasses approximately 500 unique ECG parameters. Finding the optimal parameters can be done through statistical feature selection methods in which an algorithm is trained to find the parameters that best predict a certain binary event, *e.g.* presence of LVH, or death. The selected A-ECG parameters can be expressed as a score, indicating the likelihood of having an event. The score can be modeled to range from 0–100%, where a higher score is associated with a higher likelihood of event. Importantly, previously created A-ECG scores have been shown to

be both more sensitive and more specific at identifying disease compared conventional ECG criteria (4). An appropriate feature selection strategy is necessary in order to allow facilitation of data understanding and visualization, reduced training and utilization times, reduced storage management, and avoiding overly complex and overfitted prediction models (103).

Figure 2.13. Fitting of binary classification

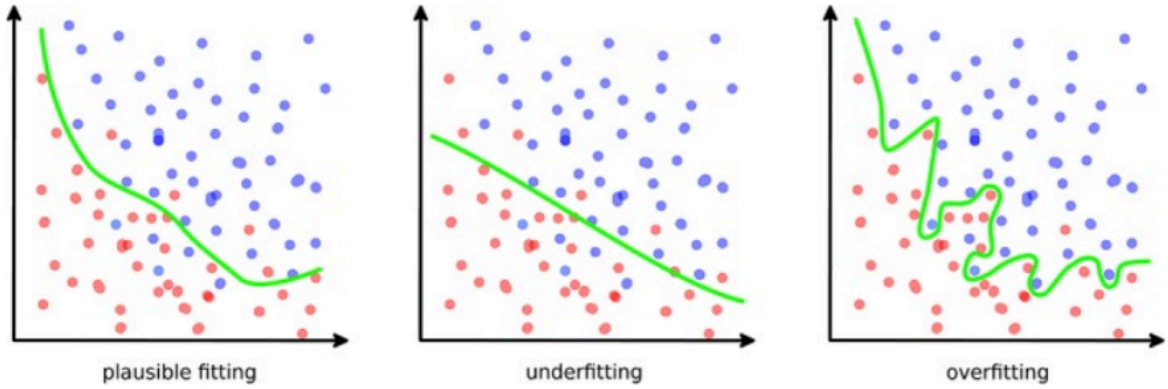

Figure 2.13: *Concept of model regularization to fit a binary classification, here to separate the blue dots from the red dots. Depending on the degree of the polynomial function, the fitting can be; plausibly fitted, underfitted, or overfitted, respectively. In mathematics, and statistics, model regularization is used to add information to a model, such as a penalty, to obtain a plausibly fitted classification while preventing overfitting. Reproduced from Galbusera, et al (104), with permission.*

Feature selection can be performed forwards or backwards. Forward selection is a technique whereby one starts with an empty model, *i.e.* no parameters, and lets the model try parameters, one at a time, that correlate best with the event. Subsequently, the remaining candidate parameters are tried to see which one adds the most predictive performance. This continues until a specified number of parameters are added to the model, or when no parameter adds further predictive capacity. Conversely, a backward elimination selection starts with a model with all parameters, and eliminates parameters that contribute the least toward predictive performance, one at a time. It has been argued that the forwards selection method outperforms the backwards selection method (105), and forwards selection was used within the scope of this thesis. However, backwards elimination suffers less from feature interaction since it starts with the full model and eliminates parameters that interact with the parameters that perform the best (105). The parameters are typically selected based on a variable ranking mechanism. However, a parameter that is useless by itself, can become powerfully predictive together with

another parameter, and parameters that correlate highly will be redundant for the model because no additional information is gained by adding them (103).

It is generally accepted that the number of parameters used to predict an outcome should be restrained to a maximum of one parameter per ten events (106). This approach is used to reduce the risk of an over-fitted model, as the requirement of events grows exponentially, referred to as "the curse of dimensionality" (107). When the optimal set of parameters for predicting an outcome have been selected, the accuracy and model performance is tested and evaluated.

The performance of a model is best evaluated by applying it to an independent cohort compared to those used to develop the model. As that require a lot of data, there are strategies to derive new groups of patients for the evaluation, such as k-fold cross-validation and bootstrapping, respectively. Bootstrapping, used in the studies in this thesis, is a resampling method in which the whole cohort is randomly sampled a set amount of times, resulting in different "new" groups.

2.5.1 Feature selection methods

Feature selection may be adopted when there is a limited knowledge about the significance of the parameters for a certain outcome or purpose, and stepwise regression may be used to identify the significant parameters (108). Within the scoop of this thesis, the feature selection method we adopted was stepwise forward logistic regression. In comparison to linear regression that assesses the relationship between a dependent variable and an explanatory variable (or independent variable), logistic regression compares the relationship between a binary dependent variable and an explanatory variable. A binary variable has two possible mathematical values, *e.g.* "0" and "1". This can translate to *e.g. yes* and *no*, or *survived* and *died*, and is thus suitable for outcomes analyses.

Besides logistic regression, several other feature selection methods are used in statistical modeling. Therefore, we also investigated Lasso, Ridge and Elastic net regression techniques when designing *Study IV*. Briefly, what these regression techniques have in common is that they introduce a bias in the regression in order to prevent overfitting in particular highly linearly related measures, so called multicollinearity.

2.5.2 Statistical diagnostic tests

Two major elements associated with clinical diagnostic tests are the sensitivity and specificity. Sensitivity is the proportion of sick individuals that are correctly diagnosed as sick by a test (true positives), and specificity is the proportion of healthy individuals that are correctly diagnosed as healthy by a test (true negatives). As sensitivity and specificity are proportions, confidence intervals (for proportions) can be calculated (109). Sensitivity and specificity can only be determined if the true diagnosis is known (110). Receiver operating characteristic (ROC) curves can be used to find the optimal cutoff by plotting all possible cutoffs resulting in a visual representation of the sensitivity and specificity at different cutoff. Depending on what is clinically desired with regards to the trade-off between a high sensitivity or specificity, the criteria or cutoff for a diagnostic test can be set accordingly. In a clinical setting it is common to optimize the sensitivity at the expense of a lowered specificity (111).

Table 2.1. Sensitivity and specificity

	Disease present	**Disease absent**
Positive test	True positive (TP)	False positive (FP)
Negative test	False negative (FN)	True negative (TN)

Table 2.1: *Sensitivity is calculated as TP / (TP + FN), and shows the fraction of patients with disease that are correctly diagnosed by a test. Specificity is calculated as TN / (TN + FP), and shows the fraction of patients with no disease (healthy) that are correctly diagnosed by a test.*

Bayes' theorem involves an *a priori* analysis used to decide the probability of an event. A patient may present with a history and clinical findings suggesting a high risk of having an event, *e.g.* LVH. Even though a certain diagnostic test may suggest that no disease is present in the patient, the result should be interpreted with caution based on clinical status, or vice versa. In addition to sensitivity and specificity, predictive values are used to evaluate the accuracy of the diagnostic test. The positive predicate value (PPV) is the proportion of positive test results that are truly positive, and the negative predictive value (NPV) is the proportion of negative test results that are truly negative.

3 AIMS

The overall aims of this thesis were to investigate the diagnostic and prognostic ability of A-ECG measures in heart disease, using CMR as the gold standard for disease.

The specific aims for each study were:

I. To investigate how LVMI and diffuse myocardial fibrosis, measured as ECV, influence the ECG patterns commonly interpreted as LVH.

II. To investigate electrocardiographical differences in LVMI and GTI by creating A-ECG scores for increased LVMI and GTI, respectively, and compare to conventional ECG criteria for LVH.

III. To define LVER based on the deviation from normal angles in the VCG, and compare the diagnostic and prognostic value of LVER to conventional ECG LVH criteria.

IV. To create ECG and CMR prognosis scores, respectively, to compare the prognostic value of the scores, and to investigate to what extent the ECG score can be explained by CMR measures.

"Biomedical statistics is the poetry of biomedical science"

– Erik B. Schelbert

4 MATERIALS AND METHODS

4.1 STUDY POPULATIONS

In all four studies, the study population consisted of retrospectively identified patients referred for a clinical CMR imaging scan at the University of Pittsburgh Medical Center (UPMC), PA, USA. In addition, *Study III* included patients who had undergone cardiac imaging at one of the seven following sites: Lund University Hospital, Lund, Sweden; Brooke Army Medical Center, San Antonio, TX, USA; Texas Heart Institute, TX, USA; the University of Texas Health Sciences Center, San Antonio, TX, USA; the University of Texas Medical Branch, Galveston, TX, USA; St. Francis Hospital, Charleston, WV, USA; and the Universidad de los Andes, Mérida, Venezuela (4). *Study III* also included healthy volunteers from NASA's Human Test Subject Facility, Houston, TX, USA; the Universidad de los Andes, and Lund University Hospital (4).

The study patients from UPMC partially overlapped among the studies, but the patients in *Study II* were included according to more strict criteria than those in *Study III* and *IV*, and the patients in study I were more strictly identified than those in *Study II*. All study participants provided informed consent, and all studies were approved by the local institutional review boards.

4.1.1 Study I

To avoid ECG confounders beside LVMI and ECV, the study population in Study I consisted of carefully selected patients from a database of patients referred for a CMR scan at UPMC between year 2010 and 2014. Inclusion criteria were an ECG with sinus rhythm with a heart rate <100 beats/min acquired within 30 days of CMR. Exclusion criteria included atrial fibrillation or flutter, bundle branch- or fascicular block, abundant premature atrial contractions, abundant premature ventricular contractions (bigeminy or trigeminy), paced rhythm, treatment with digitalis, previous MI or non-ischemic cardiomyopathy by LGE-CMR, previous cardiac surgery, pathologic stress perfusion CMR, cardiac amyloidosis, severe valvular disease by CMR, significant coronary artery stenosis by invasive angiography, EDVI >120 g/m^2, and BMI <18 or >30 kg/m^2. Because the aim of the study was to investigate how LVH-associated ECG parameters were affected by ECV and LVMI respectively, we aimed to include subgroups of equal size with all combinations of normal or increased ECV and LVMI, respectively. In a database of 1707 patients, we first applied inclusion and exclusion criteria

which yielded a cohort of 537 eligible patients. Next, we aimed to select n=20 patients with each combination of normal or increased ECG and LVMI, respectively. However, due to a shortage of patients eligible for the fourth subgroup, only 17 were available. Thus, a total of 77 patients were ultimately included in Study I, as shown in Figure 4.1.

Figure 4.1. Flowchart of patient selection in Study I

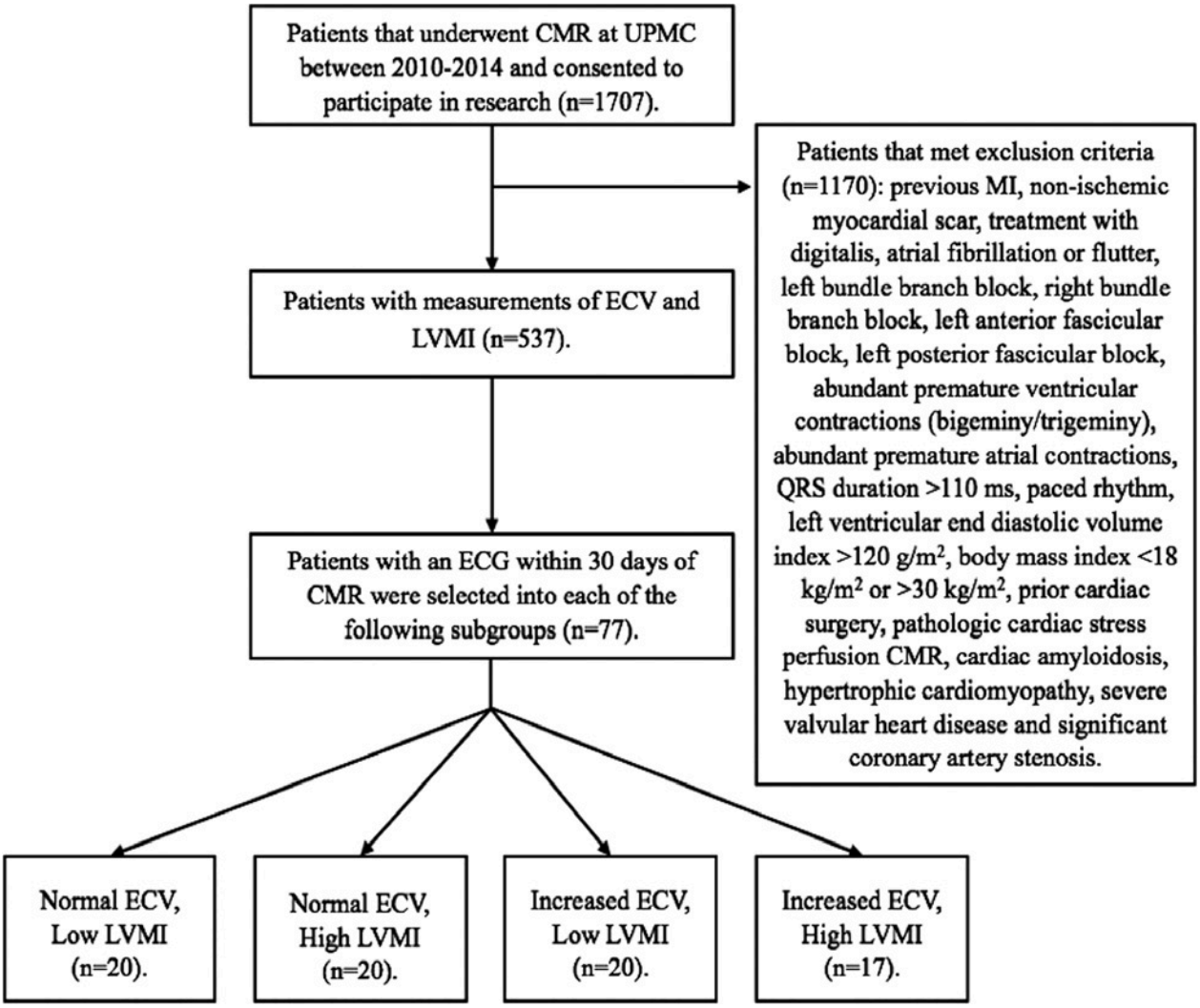

Figure 4.1: *The flow chart shows the patient selection algorithm in Study I. In a database of 1707 patients, 573 patients were eligible for the study. To investigate the study hypothesis, a total of 77 patients were ultimately included in the study. The cut-off separating normal from increased myocardial extracellular volume fraction (ECV) was 28.5%, and the cutoff separating low from high left ventricular mass index (LVMI) was 55 g/m². Figure reproduced from Study I with permission.*

4.1.2 Study II

The patients in *Study II* were identified retrospectively from the UPMC database. Inclusion criteria were an ECG with sinus rhythm acquired within 30 days of a contrast-enhanced CMR including measures of LVEDV and LVM. The following potential ECG confounders were excluded: heart rate ≥100 beats/min, QRS duration ≥120 ms, atrial fibrillation or flutter, abundant premature atrial or ventricular beats (bigeminy or trigeminy), bundle branch blocks, treatment with digitalis, and inadequate ECG records. The following CMR confounders were excluded: previous MI or non-ischemic myocardial scar by LGE-CMR, dilated or hypertrophic cardiomyopathy, severe valvular disease, amyloidosis, and significant coronary artery stenosis by stress perfusion CMR. Lastly, the following clinical parameters were excluded: previous revascularization, and any prior cardiac surgery. From a database of 1828 patients, 485 patients were eligible for the study.

4.1.3 Study III

Study III consisted of four sub-cohorts: 1) healthy volunteers to define sex-specific normal values for LVER (Healthy-Derivation cohort, n=921); 2) a separate set of healthy volunteers used to evaluate the study measures (Healthy-Validation cohort, n=461); 3) clinical patients with at least moderate LVH by cardiac imaging to evaluate the study measures (Imaging-LVH cohort, n=225); and 4) clinical patients referred for CMR imaging who also had follow-up data on all-cause death or hospitalization for heart failure, to evaluate the diagnostic and prognostic value of the study measures (Clinical-Consecutive cohort, n=783).

The three sites from where the healthy volunteers were identified have been described previously. In summary, all healthy volunteers had no evidence of cardiovascular or other systemic disease based on a negative history and a physical examination. Furthermore, they were asymptomatic, and had a clinically normal conventional ECG. Asymptomatic volunteers who were active smokers, or received treatment for hypertension or diabetes were excluded. The Imaging-LVH cohort was included from seven different sites, as described previously. In brief, inclusion criteria included an ECG with a QRS duration <120 ms acquired within 30 days of the cardiac imaging examination, and at least moderate LVH according to the clinical assessment of the reporting imaging physician or the guidelines of the American Society of Echocardiography (112). Exclusion criteria were non-sinus or paced rhythm, right or left bundle branch block, pre-excitation, incomplete ECG records, and imaging findings of a

predominant cardiac pathology other than LVH, such as MI or non-ischemic cardiomyopathy, and moderate or greater valvular disease by echocardiography.

The Clinical-Consecutive cohort was identified from the UPMC database of 1828 consecutive clinical patients who underwent a CMR at UPMC between 2008 and 2017, and had a follow-up time until April 2018. A total of 783 patients met all inclusion but no exclusion criteria. Exclusion criteria were atrial fibrillation or flutter, paced rhythm, abundant premature ventricular contractions (bigeminy/trigeminy), hypertrophic cardiomyopathy, congenital heart disease, Takotsubo cardiomyopathy, siderosis, amyloidosis, Fabry's disease, and poor CMR image quality.

4.1.4 Study IV

The fourth study consisted of the same patients (n=783), and with the same inclusion and exclusion criteria, as the Clinical-Consecutive cohort in *Study III*.

4.2 ECG ACQUISITION AND ANALYSIS

Standard 12-lead ECGs were recorded under clinical conditions using the local ECG machines. ECGs were typically recorded on a GE ECG machine and stored into the digital database (MUSE® Cardiology Information System, Version 8.0 SP2, GE Healthcare, Chicago, IL, USA). Clinical ECGs were recorded for a duration of 10 seconds, and at a sample rate of 250 Hz or 500 Hz. In *Study III*, the healthy volunteers and patients in the Imaging-LVH cohort had 5-minutes ECG recordings sampled at 1000 Hz. All ECGs were exported from the respective databases into anonymized .xml files with coded subject identification. The digital semi-automatic A-ECG software CardioSoft® (NASA, Johnson Space Center, Houston, TX, USA) was used to analyze all ECG files.

4.2.1 Conventional ECG LVH measures

A-ECG analysis includes measures of conventional P-, QRS- and T-wave amplitudes, durations, and axes. Conventional ECG criteria for LVH are based on increased QRS amplitudes and durations. In Study I-III we investigated the following established criteria, and all measures were performed and calculated digitally:

1. Sokoloy-Lyon index, defined as the sum of the the larger R wave in lead V5 (R_{V5}) or R_{V6} and S_{v1} voltage, where LVH is defined as a sum >3.5 mV (113).
2. Cornell voltage, defined as the sum of R_{aVL} and S_{V3} voltage, where LVH is defined as sum >2.0 mV for women and >2.8 mV for men (70).
3. Cornell voltage product, defined as the product of the Cornell voltage and the QRS duration, where LVH is defined as ≥244mV•ms (114).
4. The longest QRS duration in any lead, defined as the beginning of the Q-wave to the end of the S-wave, where LVH was defined as a QRS duration ≥100 ms (115).

4.2.2 Vectorcardiographic measures

All VCGs were derived from the 12-lead ECG using Kors' transform (3, 54). The VCG shows the spatial direction and magnitude of the electrical vector in the three-dimensional space, for each of the three perpendicular two-dimensional planes, namely the frontal, horizontal, and (left) sagittal plane. From this three-dimensional space, several different VCG measures were obtained, including:

- The direction and magnitude of the QRS loop and T loop vector in space, expressed as elevation or azimuth angles from a predefined plane.
- The morphologic configuration of the QRS loop and T loop, such as Tavplan (116, 117).
- The direction and duration of vectors and whole vector loops.
- The QRS-T angle, defined as the difference between the mean or peak angles of the QRS and T loop.

The elevation angle is the angle between the vector and the respective plane. Forward directions are defined as 0–180°, and backward directions are defined as 0– -180°. When observing a torso in the upright position from the front, 0° is defined as a vector pointing to the left in the frontal plane, and as a vector pointing to the back in the horizontal and left sagittal plane. P loop measures were not used within the scoop of this thesis since 10-second ECG recordings are not long enough to achieve an adequate signal-to-noise ratio for deriving P loops.

4.2.3 QRS wave and T wave complexity measures.

Mathematical SVD was used for detailed studies of QRS and T wave complexity. This rendered eigenvectors 1 through 8 for the respective waves.

4.3 CMR ACQUISITION AND ANALYSIS

All CMR acquisition was performed at UPMC CMR Center, PA, USA, and images were analyzed using the local Leonardo work station (Siemens Healthcare, Erlangen, Germany). CMR images were acquired using a scanner with a field strength of 1.5 T (Magnetom Espree, Siemens Healthcare, Erlangen, Germany) and a 32-channel phased array surface coil.

4.3.1 Dimensions, volumes, and late gadolinium enhancement

The CMR exams included standard breath-held segmented cine imaging with a steady-state free precession (SSFP) sequence. Short-axis stacks were acquired and used to measure LV mass, volumes, and ejection fraction in end-systole and end-diastole. Typical acquisition parameters were field of view 360x270 mm^2, matrix size 256x128 pixels, and slice thickness 6 mm. Ten minutes after a 0.2 mmol/kg intravenous bolus injection of gadoteridol (Prohance, Bracco Diagnostics, Princeton, NJ, USA), LGE imaging was performed using a phase-sensitive inversion recovery (PSIR) pulse sequence. If a patient could not breath-hold properly, a single-shot motion corrected PSIR sequence was used (118, 119). Global wall thickness, defined as the mean wall thickness of the whole left ventricle in end-diastole, measured in millimeters, was calculated according to previously validated methods (27) as:

$$GT = 0.05 + 1.60 \cdot LVM^{0.83} \cdot LVEDV^{-0.49}$$

4.3.2 Quantification of extracellular volume fraction

Quantitative T1 maps were acquired using an ECG-gated single-shot-modified Look Locker inversion recovery sequence (MOLLI), and the maps were used to calculate ECV. Native T1 maps were acquired followed by a bolus injection of a gadolinium-based contrast agent, and acquisition of post-contrast T1 maps. T1 was measured in areas without LGE, and in the middle third of the myocardium to avoid partial volume effects. ECV was calculated as:

$$\text{ECV} = \lambda \cdot (1 - \text{hematocrit})$$

where $\lambda = \Delta R1_{myocardium} / \Delta R1_{bloodpool}$ and $\Delta R1 = 1/T1_{postcontrast} - 1/T1_{precontrast}$ (90). ECV in the blood was calculated from a circular region traced in the middle of the blood pool to avoid partial volume effects from papillary muscles. The final myocardial ECV values were averaged from basal and mid-ventricular short axis slices. Apical slices were not used to calculated ECV due to obliquity between the image plane and myocardium, which could introduce partial

volume effects (18). Hematocrit measures were acquired on the day of CMR and analyzed in the clinical laboratory.

Figure 4.2. Distribution of Gd contrast and calculation of ECV

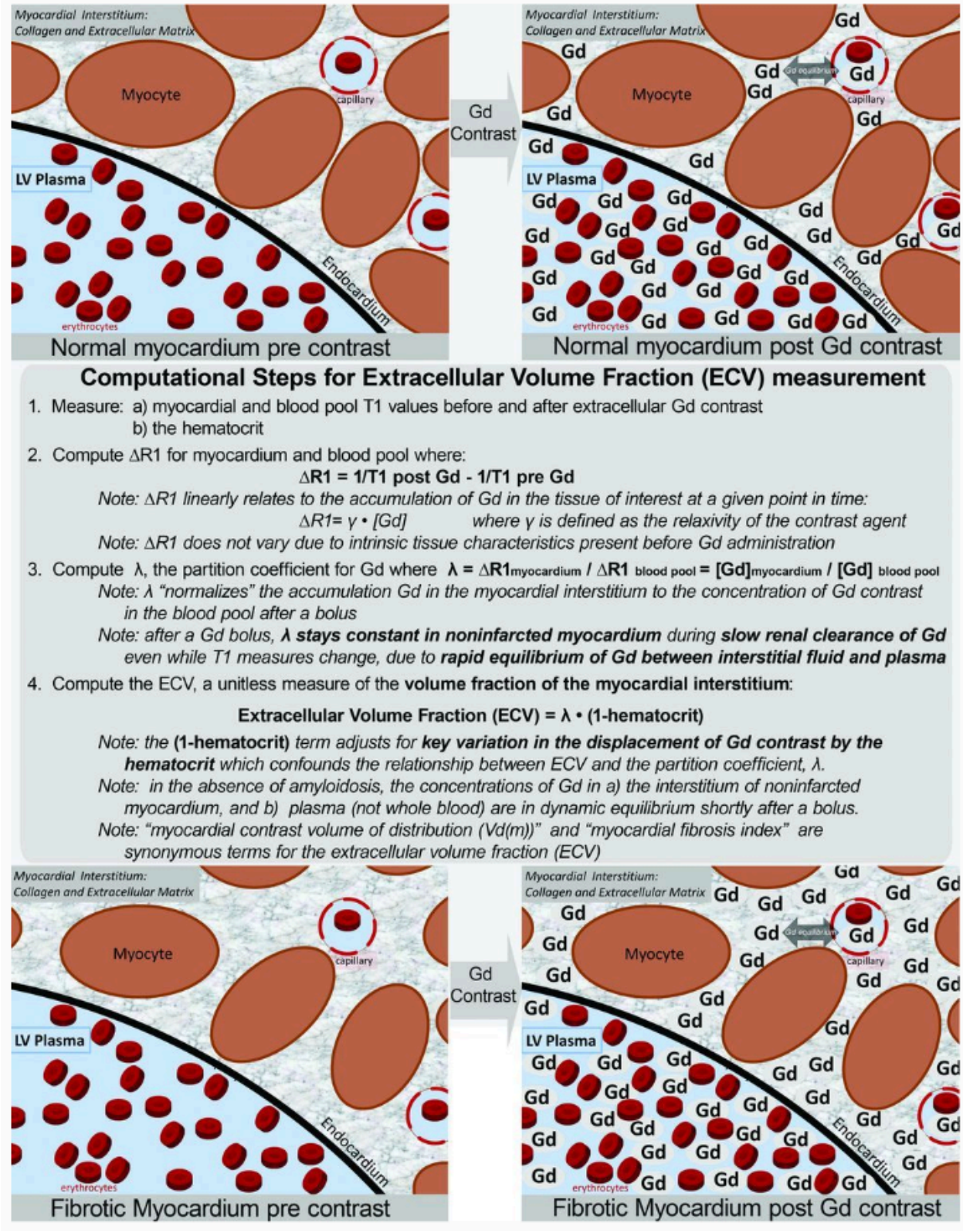

Figure 4.2: *Gadolinium-based contrast agents (Gd) distribute freely in the extracellular space and do not enter living cells. Myocytes, myocardial capillaries, extracellular matrix with*

collagen, plasma, erythrocytes, and Gd molecules are illustrated in the figure. The upper panel shows normal myocardium before and after contrast, and with a normal distribution of Gd in the myocardial interstitium after administration. The lower panel shows fibrotic myocardium before and after contrast, and with an increased distribution of Gd in the myocardial interstitium after administration. The middle panel shows the computational steps for extracellular volume fraction measurement from T1 images. Figure reproduced from Wong, et al (120), with permission.

4.3.3 Quantification of global longitudinal strain

GLS was analyzed using a semi-automated tissue feature tracking software (CVi42, Circle Cardiovascular Imaging Inc., Calgary, Canada). Epicardial and endocardial borders were traced manually in 2-, 3-, and 4 chamber end-diastolic images. Strain analysis tracings were inspected visually throughout the cardiac cycle, and if tracings deviated from myocardial movement, manual adjustments were made.

4.4 ECHOCARDIOGRAPHIC ANALYSIS

In *Study III*, echocardiography was used to diagnose LVH besides CMR. By echocardiography, LVH was defined as moderate or greater as reflected in the clinical report, according to the guidelines of the American Society of Echocardiography (112).

4.5 STATISTICAL ANALYSIS

In Study I, statistical analyses were performed using SPSS version 23 (IBM Corp, Armonk, NY, USA). In *Study II-IV*, statistical analyses were performed using R version 3.4.3 (R Foundation for Statistical Computing, Vienna, Austria) with, among others, packages dplyr (121) for data transformation, and ggplot2 (122) for data visualization. A p-value <0.05 was considered statistically significant.

The Kolmogorov-Smirnov test was used to test whether variable distribution deviated from normal distribution. Differences in normally distributed data were compared with the unpaired Student's t test, or analysis of variance (ANOVA), as appropriate, and described using mean

and standard deviation (SD). Differences in non-normally distributed data were compared using Mann-Whitney U test, or Kruskal-Wallis test, as appropriate, and described using median and interquartile range (IQR). Differences in proportional data were compared using Chi-squared test, and described as the quantity and as a percentage. Linear correlations were evaluated using Pearson's correlation coefficient (r), and expressed as its square (R^2). Univariable and multivariable Cox regression (proportional hazards regression) analyses were used to calculate hazard ratios (HR) for outcome and survival analyses, and Kaplan-Meir plots were created for endpoint visualizations.

The diagnostic and prognostic scores for a binary outcome used in *Study II* and *IV* were derived using continuous A-ECG measures and stepwise forward logistic regression. A maximum of one parameter per ten events was accepted for the scores (106). To determine the diagnostic accuracy of the derived scores, the area under the ROC curve (AUC) was calculated and bootstrapped 2000 times to obtain ninety-five percent confidence intervals (95% CI). When more than one score was derived, the score with the highest AUC was chosen. The Youden index (123) was used to identify the cut-off for the scores that optimized sensitivity and specificity. The logistic scores were constructed to show a likelihood of event, ranging from 0–100%, and calculated from the logistic regression as:

$$Likelihood\ of\ event = \frac{1}{1 + e^{numerical\ score\ result}} \cdot 100$$

where the numerical score result is the calculated value for each study patient based on their A-ECG measures. In *Study II*, DeLong's test (124) was used to compare the AUC between different scores and measures. In *Study IV*, besides sensitivity and specificity, the positive predictive value (PPV) and negative predictive value (NPV) were calculated to evaluate the performance of the score. Lastly, a recently published prognostic ECG score by Aro, *et al* (125), (Aro ECG risk score) was also investigated which was defined as the fulfillment of four or more of the following criteria: QRS duration >110 ms, QTc time > 450 ms in men and > 460 ms in women, heart rate >75 bpm, frontal plane QRS-T angle >90°, T_{peak}–T_{end} duration >89 ms, electrocardiographic LVH, delayed QRS transition zone, or a delayed intrinsicoid deflection, assessed from the 12-lead ECG.

“Expect nothing and appreciate everything”

– Unknown

5 RESULTS AND DISCUSSION

We investigated if we could find an explanation regarding why the ECG criteria for LVH are poor, and if ECG diagnosis of LVH could be improved. **In *Study I*** we found that diffuse myocardial fibrosis is associated with reduced ECG voltage amplitudes, which are typically used to diagnose LVH. This provided mechanistic insight which can, in part, explain the limited sensitivity of the ECG for detecting increased LV mass. Based on these results, we sought to investigate whether A-ECG parameters could be used to improve the ECG-based diagnosis of LVH. **In *Study II*** we found that A-ECG parameters could better detect LVH than conventional ECG LVH criteria. We further found electrocardiographic differences between hypertrophy with either increased LVMI or GTI, or a combination of both. **In *Study III*** we chose to use the term LVER in order to emphasize our focus on electrical changes considered associated with LVH, but which can occur independently of anatomical LVH. We found that LVER, defined as a spatial peaks QRS-T angle greater than its normal distribution in a healthy population, improved the diagnosis of LVH compared to conventional ECG LVH criteria. Furthermore, LVER also provided prognostic information. With those results, we sought out to optimize an ECG-score for survival. **In *Study IV*** we found that a new simple ECG score predicted outcomes beyond known powerful prognostic CMR measures.

5.1 THE IMPACT OF DIFFUSE MYOCARDIAL FIBROSIS UPON ECG MEASURES OF LEFT VENTRICULAR HYPERTROPHY

Study I was a mechanistic study designed to investigate how diffuse myocardial fibrosis, measured as ECV, affects voltage measures and QRS duration, on the conventional ECG interpreted as LVH. Diffuse myocardial fibrosis was previously only diagnosed through invasive biopsy, but has been histologically validated to be strongly correlated to T1 measurements by CMR (30, 34, 126-129). Despite the central diagnostic role of the ECG in cardiology, no data existed on the contributions of diffuse myocardial fibrosis to the ECG changes in LVH. The diagnostic performance of conventional ECG LVH criteria vary greatly (68), and it may be due to confounding factors such as diffuse myocardial fibrosis.

To investigate the effects of diffuse myocardial fibrosus upon ECG measures of LVH, we studied a carefully selected group of patients without any other apparent clinical, CMR, or ECG co-morbidities that could potentially influence the ECG besides diffuse myocardial fibrosis and

increased LV mass. See Figure 4.1 for a detailed list of exclusion criteria. The results showed a positive relationship between LVMI and the investigated ECG measures, and an inverse relationship between ECV and the investigated ECG measures.

Figure 5.1. Linear correlations between LVMI, ECV and ECG LVH measures

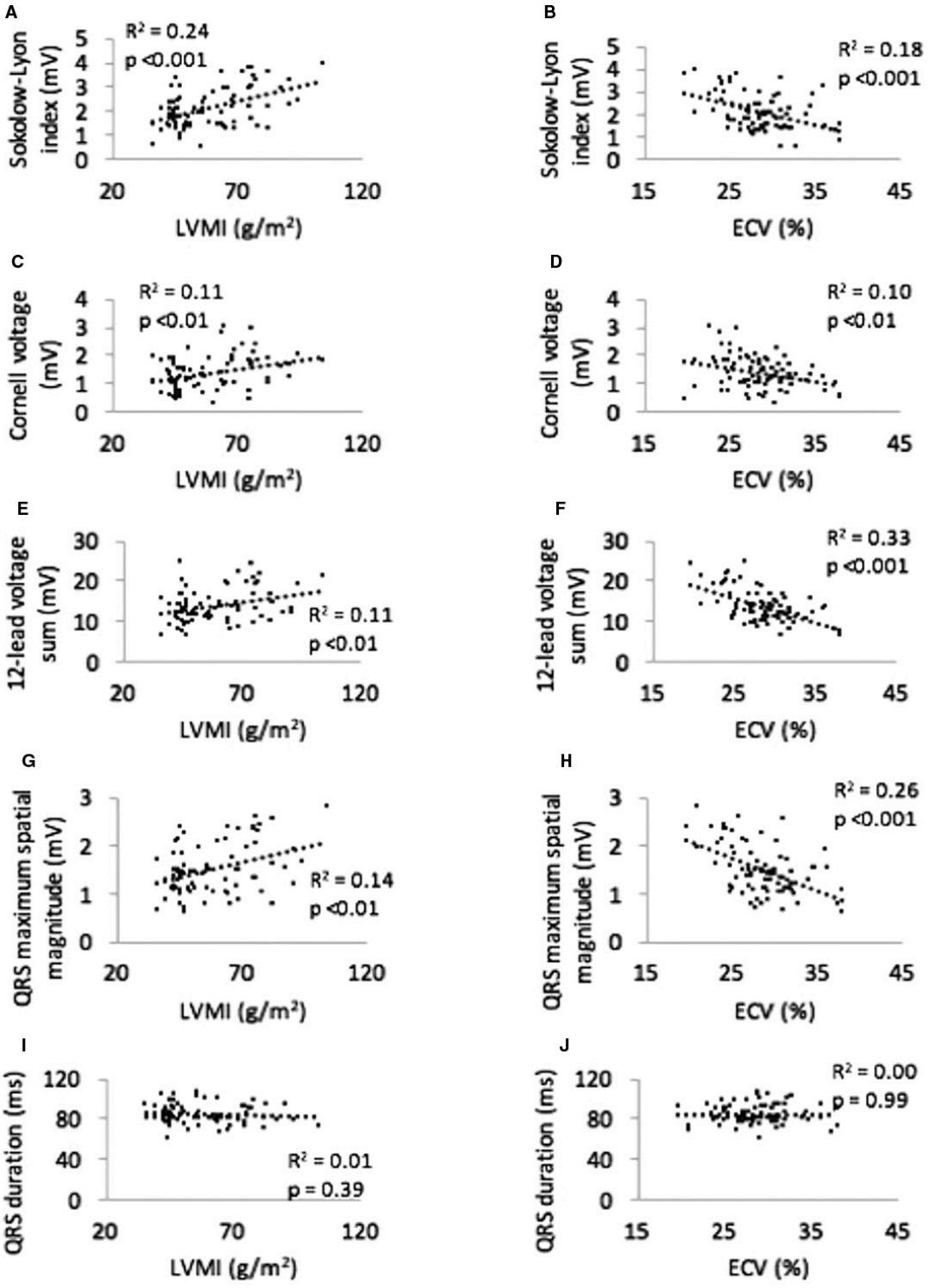

Figure 5.1: *Linear correlations between ECG measures Sokolow-Lyon index, Cornell voltage, 12-lead voltage sum and QRS maximum spatial magnitude, and LVMI and ECV, respectively. Note that LVMI is positively correlated with all voltage measures (subfigures A, C, E, G), whereas ECV is inversely correlated with all voltage measures (subfigures B, D, F, H). The QRS duration was neither correlated to LVMI nor ECV. Figure reproduced from Study I, with permission.*

A plausible physiological explanation for the results may be that increased LVMI gives rise to longer and larger living electrical activation patterns with increased QRS amplitudes (78). However, in LVH there is a process beyond the increase of mass, including myocyte apoptosis, changes in electrical phenotype, and alterations in the composition and quantity of the extracellular matrix that may interfere with QRS voltage (78). Furthermore, an increase in ECV, consisting mostly of collagen, may serve as an electric insulator and decrease the voltage recorded by ECG. This phenomenon has been observed in other cardiac conditions such as infiltrative cardiomyopathies, and after myocardial infarction (130, 131). However, patients with such diagnoses were excluded from the study. We did not find any correlation between QRS duration and increased LVMI, as have been reported in previous studies (132-135).

5.2 ADVANCED VS CONVENTIONAL ECG IN LVH DIAGNOSIS

To our knowledge, previous ECG LVH studies have not investigated whether different LVH sub-patterns have different electrocardiographic characteristics. An established classification of LVH commonly used in imaging studies divides LVH into the three patterns: concentric remodeling, eccentric hypertrophy and concentric hypertrophy, respectively, based on LVMI and some measure of relative wall thickness, *e.g.* GTI (26). Therefore, the electrocardiographic differences in increased LVMI and GTI, respectively, were investigated. Similar to *Study I*, we excluded patients with potential CMR, ECG, or clinical confounders that could possibly affect the ECG. Even though ECV affects the ECG, as was found in *Study I* (75), patient with increased ECV were not excluded. The feature selection method stepwise forward logistic regression was employed to identify A-ECG parameters that would comprise a diagnostic score that could best identify increased LVMI, and GTI, respectively. We found that different patterns of LVH indeed differed in their electrocardiographic manifestation by A-ECG.

The increased LVMI A-ECG score, and increased GTI A-ECG score had a higher AUC than all conventional ECG LVH parameters in diagnosing increased LVMI, and GTI, respectively.

Figure 5.2. AUC for scores for increased LVMI and GTI

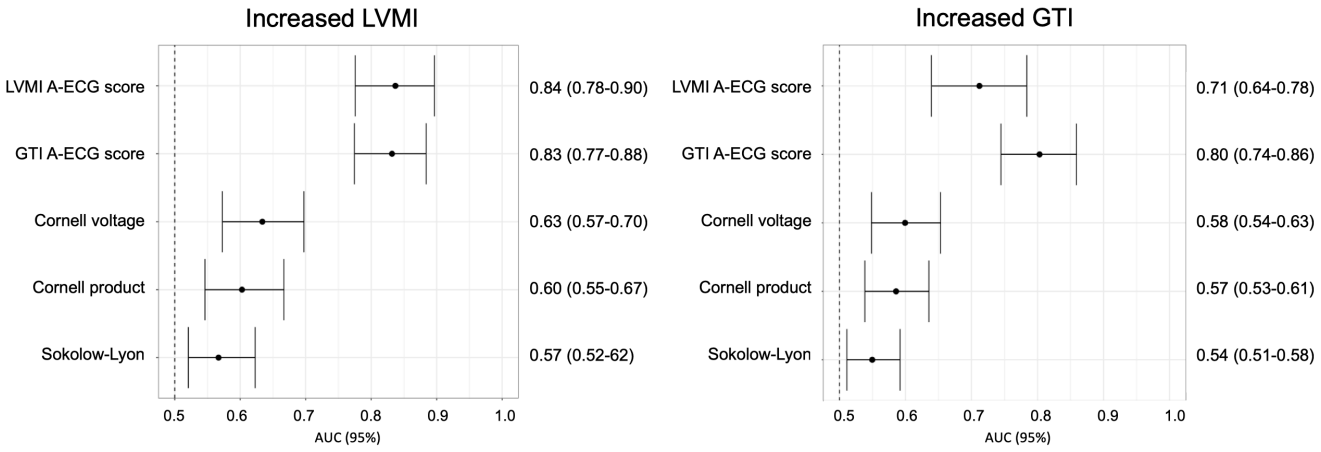

Figure 5.2: *The area under the curve (AUC) for the increased LVMI A-ECG score and GTI A-ECG score, respectively, in detecting increased LVMI and GTI, respectively. The A-ECG scores had a higher AUC than Cornell voltage, Cornell product and Sokolow-Lyon index for detecting increased LVMI and GTI, respectively. Interestingly, the GTI A-ECG score could detect increased LVMI on par with the dedicated LVMI A-ECG score. Figure reproduced from Study II with permission.*

Compared to conventional ECG LVH criteria (Sokolow-Lyon index, Cornell voltage, and Cornell voltage product) which are based on increased voltage amplitudes and prolonged QRS durations, the diagnostic A-ECG parameters for detecting increased LVMI, and GTI also included VCG parameters and measures of QRS wave complexity. It may be that these measures have a more global and varied diagnostic performance than solely increased voltages. Essentially all measures that were incorporated into the diagnostic scores, as presented in Table 5.1, have previously been studied in ventricular hypertrophy (64, 136-142). If patients with increased ECV had been excluded, additional, or different, voltage measures may have been significant for the diagnosis. However, as the study population was selected from patients undergoing a clinically indicated CMR scan, the results reflect a general group of patients with LVH, which was the investigated group of interest. The results give further insight into the limited sensitivity of the conventional ECG based on the different electrical properties captured by A-ECG. The results also highlight diagnostic information present in the ECG that can improve clinical LVH diagnosis.

Table 5.1. A-ECG parameters in the increased LVMI and GTI scores

ECG parameter		Z-value	*p* value	AUC (95% CI)
Increased LVMI score				
1)	The area of the QRS vector magnitude (mV•s)	6.0	<0.001	0.84 (0.78-0.90)
2)	The QRS loop area outside the left lower quadrant in the left sagittal plane (%)	-3.3	<0.001	
3)	T wave amplitude in lead aVR (μV)	-3.2	0.001	
4)	QTc (ms)	2.7	0.007	
Increased GTI score				
1)	6th Eigenvalue (singular value) of the QRS	4.4	<0.001	0.80 (0.74-0.86)
2)	The bulginess of T vector loop (mV)	4.2	<0.001	
3)	The azimuth of the maximum QRS magnitude in the left sagittal plane (radians)	3.5	<0.001	
4)	T wave amplitude lead I (μV)	-3.5	0.002	
5)	The latitude of the polar vector (degrees)	-2.8	0.006	

5.3 LEFT VENTRICULAR ELECTRICAL REMODELING – DIAGNOSIS AND PROGNOSIS BEYOND ECG LVH

Electrical and anatomical properties of the heart are fundamentally different. Importantly, both properties are important as they predict prognosis independently of each other (24). Although A-ECG measures have a higher diagnostic performance compared to conventional ECG for diagnosing LVH as determined by imaging (143), there are still several important and related issues. First, the limited diagnostic performance of ECG criteria for detecting anatomical changes present in LVH may likely be related to the inherent differences between

electrophysiology and anatomy. Second, the term LVER has been suggested to be more appropriate when referring to the electrical changes present in LVH (144, 145). We therefore considered it a reasonable approach to define LVER in terms of electrical changes in the myocardium based on deviation from normality observed in healthy individuals, rather than based on a non-electrical anatomical marker such as LVH. *Study III* examined the spatial peaks QRS-T angle in healthy individuals, patients with LVH, and clinical consecutive patients. The QRS-T angle can be derived from a digital 12-lead ECG, but it can also be manually estimated from a paper-based 12-lead ECG (146).

In *Study IV*, LVER was defined as greater than the sex-specific 97.5th percentile of normal for the VCG spatial peaks QRS-T angle based on healthy volunteers (Healthy-Derivation cohort, n=921), resulting in an angle ≥40° in females and ≥55° in males. LVER was absent in nearly everyone in a separate cohort of healthy volunteers (Healthy-Validation cohort, n=461). Furthermore, LVER was present in nearly all subjects with an isolated LVH (Imaging-LVH cohort, n=225). See Figure 5.3 for the sensitivity and specificity for the LVER criterion and conventional ECG criteria in the respective cohorts. In the Clinical-Consecutive cohort, however, the sensitivity and specificity of the LVER criterion to diagnose LVH was not as excellent as in the prior cohorts. This may be due to confounding co-morbidities in the clinical cohort, such as non-ischemic or ischemic myocardial scar, or other co-morbidities since they were referred for a clinical CMR scan. Interestingly, LVER was also present in patients in the Clinical-Consecutive cohort that did not have LVH. This illustrates that LVER identifies an electrical remodeling process beyond LVH, and may thus be missed by anatomical imaging. We found that the QRS-T angle improved the diagnosis of LVH beyond conventional ECG criteria, in accordance with previously publishes results (147).

Patients with LVER had a worse prognosis with regards to the combined end-point survival free from hospitalization for heart failure and death compared to those without. The same was found in all investigated conventional ECG LVH criteria except the Sokolow-Lyon index. This study showed an improved diagnostic performance, and a prognostic performance beyond that of conventional ECG LVH criteria. Furthermore, it highlighted the importance of separating electrical and anatomical terminologically, for both diagnostic and pedagogical advantages.

Figure 5.3. LVER and conventional ECG criteria in LVH

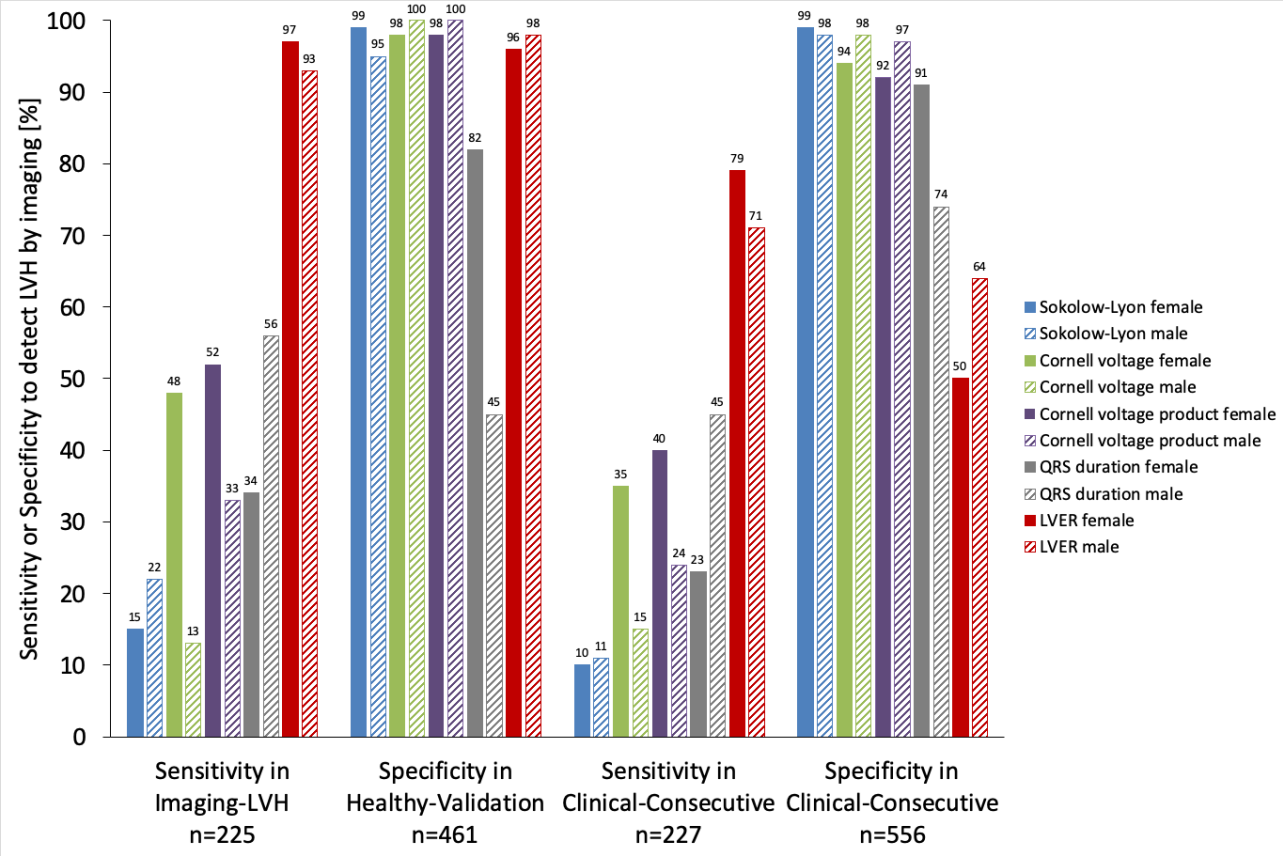

Figure 5.3: *The sex-specific sensitivity and specificity of the conventional ECG measures Sokolow-Lyon index, Cornell voltage, Cornell voltage product, and QRS duration, respectively, and of the LVER criterion for detecting imaging-verified LVH. LVER was defined as spatial QRS-T angle ≥40° for females and ≥55° for males, and had a higher sensitivity for LVH in both the Imaging-LVH and Clinical-Consecutive cohort compared to the other ECG measures ($p<0.05$ for all). Among females in the Healthy-Validation cohort, the LVER criterion had a higher specificity than the QRS duration ($p<0.001$), did not differ from that of Cornell voltage or Sokolow-Lyon index ($p>0.05$ for both), and had a lower specificity than Cornell product ($p<0.05$) in detecting LVH. Among males the Healthy-Validation cohort, the LVER criterion had a higher specificity than the QRS duration ($p<0.001$), did not differ from Sokolow-Lyon index ($p>0.05$), and was lower than Cornell voltage and Cornell voltage product ($p<0.05$ for both). In the Clinical-Consecutive cohort, all conventional ECG measures had a higher specificity than the LVER criterion ($p<0.05$ for all) despite its excellent specificity in the Healthy-Validation cohort. This suggests possible electrical identification of disease by LVER in patients who do not fulfill imaging criteria for LVH.*

5.4 ADVANCED ECG AND PROGNOSIS

The VCG spatial peaks QRS-T angle derived from the VCG was found to predict prognosis. Therefore, we set out to investigate if other A-ECG parameters have prognostic power, and if we could create an ECG prognosis score for the combined endpoint of hospitalization for heart failure and death. In *Study IV*, we adopted the same statistical methods as in *Study II*, *i.e.* stepwise forward logistic regression to identify ECG parameters for the score. Event after one year of CMR was chosen for investigation as it is at a time point when both a clinically and statistically meaningful number of events would be observed. A CMR prognosis score for 1-year event was also derived, and compared to the ECG prognosis score. Besides stepwise forward logistic regression, logistic models with a Ridge, Lasso, or Elastic Net penalty, respectively, were also evaluated for ECG feature selection. Furthermore, an A-ECG score based on Cox regression for continuous was also created to include the information in the events that occur continuously.

The final A-ECG prognosis score for 1-year event included two parameters: 1) the frontal QRS-T angle (degrees), and 2) the QTc (Bazett (148)) duration (ms). The frontal QRS-T angle and QTc where poorly correlated (R^2=0.06, p<0.001). The A-ECG score based on Cox regression included a combination of 19 parameters (13 A-ECG parameters, and 6 conventional ECG parameters). The simpler logistic ECG score had a similar AUC (95% CI) of 0.78 (0.71–0.84) compared to the more complex A-ECG score based on Cox regression with an AUC (95% CI) of 0.77 (0.69–0.84) at one year of follow-up. Both ECG parameters included in the logistic ECG score have previously been shown to predict prognosis. The frontal QRS-T angle is the angle between the QRS and T axis in the frontal plane (resembling the three-dimensional spatial QRS-T angle). A wide QRS-T angle reflects a dispersion between the depolarization and repolarization (57), and is known to be increased as a result of myocardial disease (58). Prolonged QTc durations are associated with an increased risk of sudden death and ventricular fibrillation (149).

The prognostic models using logistic regression with a Ridge, Lasso, or Elastic Net penalty, respectively, were more complex than the two-parameter ECG score based on stepwise logistic regression, and either did not outperform it, or did not provide any meaningful magnitude of improved diagnostic performance (results not shown).

The final CMR prognosis score for 1-year event included two parameters: 1) GLS (%), and 2) ECV (%), and had an AUC (95% CI) of 0.77 (0.69–0.84). GLS and ECV were poorly correlated (R^2=0.05, p<0.001). Both CMR measures are known powerful predictors of adverse prognosis. An increase in extracellular volume fraction leads to diastolic and systolic dysfunction, as well as an increased risk of arrhythmia and mortality (17). GLS had a superior significance for prognosis compared to LVEF, in accordance with previous findings (150). Other CMR measures have previously been shown to associate with outcomes, such as LVM (101), but were not significantly associated with 1-year event in the current study. The difference may be a longer follow-up times than what we investigated (101).

Figure 5.4. Survival for ECG and CMR prognosis scores

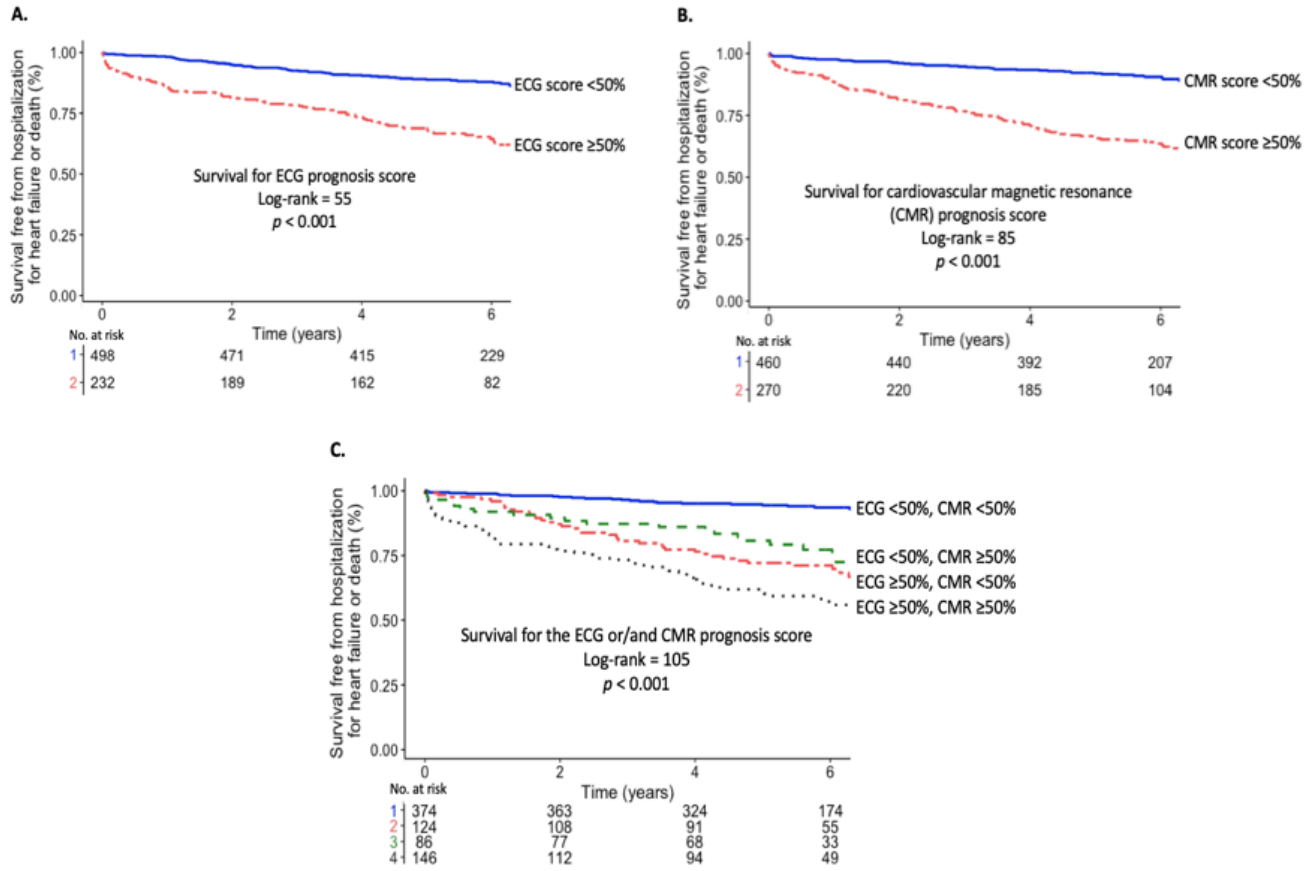

Figure 5.4: *Kaplan Meir curves showing survival free from hospitalization for heart failure or death for:* ***A.*** *patients with a normal (<50%) or increased (≥50%) ECG prognosis score,* ***B.*** *patients with a normal or increased CMR prognosis score, and* ***C.*** *patients with a normal ECG and CMR score, patients with a normal ECG score and increased CMR score, and vice versa, and patients with both an increased ECG and CMR score. Figure adapted from Study IV.*

Univariable Cox analysis showed that the CMR prognosis score had a higher univariable association with outcomes compared to the ECG prognosis score (χ^2 93, HR 2.17 [1.85–2.54], and χ^2 58, HR 1.79 [1.54–2.08], respectively, $p<0.001$ for both). Patients who had both a positive ECG prognosis score, and a positive CMR prognosis score, *i.e.* a score/probability greater than 50%, had the worst prognosis, see Figure 5.4.

The Aro ECG risk score (125) was constructed to predict sudden cardiac death and studied to specifically compare a logistic prognostic score to a point-based prognostic score. In our cohort, the Aro ECG risk score had a limited power of predicting outcomes, with an AUC of 0.65 (0.57–0.72). Discrepancies in the final end-point, and patient selection in the current and original cohort may be the reason to the lower performance of the Aro ECG risk score in our cohort. Besides the current study, the ECG has previously been compared to cardiac imaging modalities with regards to prognosis, and found to have an independent or incremental prognostic power. For instance, it has been evaluated in patients with myocardial infarction with non-obstructed coronary arteries (151), and in LVH (24, 69).

5.5 STRENGTHS AND LIMITATIONS

All four studies in this thesis were retrospective, even though the data was acquired prospectively. This may introduce selection bias. However, the aim of *Study I* and *Study II* was to study carefully selected patients which we believe were unique and important strengths to investigate the hypotheses. Furthermore, all data except the Healthy volunteers and LVH-Imaging cohorts in *Study III* was from a single university hospital in USA, and may not reflect a general global population. All ECG data was analyzed using the same dedicated semi-automatic software, which may introduce a systematic bias, but a minimal interobserver variability. The A-ECG software is not optimal for analyzing certain heart arrhythmia including atrial fibrillation or abundant premature atrial or ventricular beats, rendering results that are not applicable to such patients. Furthermore, patients with bundle branch blocks were also excluded from all studies.

In the studies investigating LVH and its electrocardiographic manifestations, only four conventional criteria were investigated, even though several have been recommended by the

American Heart Association. However, the most commonly used criteria in clinical routine were investigated, and sex-specific cut-offs were used.

The increased LVMI and GTI scores in *Study II*, and ECG prognosis score and CMR prognosis score in *Study IV* were derived and validated in the same cohort. To account for this, the AUC was bootstrapped two thousand times to obtain confidence intervals. Even so, validation in separate cohorts is necessary. Nevertheless, nearly all ECG parameters incorporated into the scores have previously been shown to be associated with prognosis. In *Study IV*, the composite endpoint of hospitalization for heart failure and all-cause death was investigated, and all-cause death may not necessarily be due to cardiac disease. However, both endpoints are unfavorable, and all events of hospitalization for heart failure were based on strict criteria. The performance of the diagnostic and prognostic scores were evaluated by bootstrapping the cohort. The bootstrapped cohorts can only include features already present in the original cohort. Therefore, patients with other features than those present in the original cohort may not benefit from the same accuracy of the derived scores.

5.6 CLINICAL PERSPECTIVES

- The ECG is a common diagnostic tool and is used in many levels of the health care system. The studies in the current thesis give insight into the limited sensitivity of voltage-based ECG criteria for detecting increased LVM. This may be due to diffuse myocardial fibrosis, or due to the different patterns of LVH. However, wherever digital 12-lead ECGs are available, the diagnostic scores from the studies could potentially be employed in the clinical software for improved diagnostics. Furthermore, the parameters in the newly proposed ECG prognosis score, namely the frontal QRS-T angle and QTc duration, are already available in clinical software, and thus the scores can easily be calculated in clinical routine. Patients with a high prognosis score may benefit from intensive risk management, surveillance, and possible therapeutic treatment, which warrants future prospective studies.

- Electrocardiographic and anatomical properties of the heart are fundamentally different phenomena. We suggest that the term LVER should be used when discussing electrical

changes present in LVH. LVER, defined as an increased spatial QRS-T angle, was hardly present in healthy individuals, widely present in LVH, and present in patients with other cardiovascular pathologies also resulting in electrical remodeling. If a digital ECG analysis is not possible, LVER can be estimated manually from a paper-based 12-lead ECG using established techniques (146), albeit probably with some compromise in accuracy and precision. Patients with LVER also had a poorer prognosis compared to those with no LVER, which warrants future studies on potential preventative treatments.

- Both electrocardiographic, functional, and anatomical properties of the heart convey independent prognostic and diagnostic information. It is therefore beneficial to assess all when possible.

6 CONCLUSIONS

Conventional ECG has repeatably been shown to lack sensitivity for LVH. A-ECG can detect LVH with an improved accuracy. As LVH is an anatomical phenomenon and the ECG records electrical phenomena, the term LVER should preferentially be used when describing and diagnosing electrical changes commonly present in LVH. Lastly, the ECG carries added prognostic information beyond that of cardiovascular magnetic resonance imaging.

The specific conclusions for each study were:

I. Myocardial mass and diffuse myocardial fiborosis had independent and opposing effects upon ECG voltage measures of LVH. This provides mechanistic insight that could explain the limitied sensitivity of the ECG for detecting increased LVM.

II. Increased LVM and GT, respectively, differed in their electrrocardiographical manifestation by A-ECG. New A-ECG scores outperform conventional ECG criteria for LVH in determining increased LVMI and GTI.

III. LVER rarely occurred in healthy volunteers, and was a mainstay of moderate or severe LVH. Furthermore, LVER was commoint evein in clinical patients without any LVH, and associated with outcomes.

IV. An ECG prognosis score predicted outcomes independently of, and beyond, CMR. Combining the results of both an ECG and a CMR prognosis score, respectively, improved overall prognostic performance.

7 ACKNOWLEDGEMENTS

I have had the privilege to meet, get to know, and work with many people since I first started doing research in 2015 as a part of my medical school thesis. It has been an amazingly fun time and experience, and I have grown as a researcher, clinician, and person. I would like to express my appreciation and gratitude to these people with big hearts…

First and foremost, I would like to thank my supervisors **Martin Ugander**, **Todd Schlegel**, **Björn Wieslander**, and **Andreas Sigfridsson**. **Martin**, for giving me the opportunity and encouragement to first travel to the USA when I was in medical school, and to pursue this PhD. Thanks for all discussions about science, and life in general, whether we were at a large international conference or at the ballet. **Todd**, for always teaching me about science and A-ECG, and for inviting me to your home to learn even more. **Björn**, for guiding me in the world of research when I was still a medical student, and for a great time in Pittsburgh, and ever since. **Andreas**, for teaching me about MRI physics in an understandable way, and for being a great research group leader. Thank you all for teaching and guiding me to becoming a more independent researcher.

To all the scientists and co-authors around the world that I have had the pleasure to work with. **Erik Schelbert**, for inviting me to your lab in Pittsburgh as a medical student and letting me explore the field of CMR and ECG, and for all our research collaborations that followed. Thanks to all the ECG enthusiast I have had the pleasure to get to know during the scientific MALT and STAFF meetings, not the least **Ljuba Bacharova**, **Kees Sweene**, **Olle Pahlm**, **Henrik Engblom**, **Staff Warren**, **Liliane Wecke**, and all the young investigators; thanks for creating a safe and creative environment to explore and grow. To **James Moon**, and **Rebecca Kozor**, for inviting me to your departments in London and Sydney, respectively, and for your collaborations. **Kenneth Caidahl**, professor in our group, for your great support and kind comments. **Selma Olsson Åkefeldt**, thank you for being a great mentor.

A huge thanks to everyone in the Karolinska CMR group, for all the good times, both at home and abroad. **Simon Thalén** and **João Ramos**, even though we have been struggling together, life is always great together with you, both in real life and on Snapchat. **Alexander Fyrdahl**, for your awesome and nerdy conversations, and technical support. **Magnus Lundin**, for making me take the train to a conference in Barcelona, and for spreading joy all around. **Jannike Nickander**, you are a great inspiration and researcher. **Fredrika Fröjdh**, and **Johan**

von Scheele, thanks for your help and for the fun times. **Daniel Loewenstein**, thanks for help with statistics. **Rebecka Johansson**, and **Adele Kastensson**, thanks for your contributions to the group. To **Kristoffer Lundbäck**, and **Ali Ilami**, for always making me laugh, especially when playing ping pong. All you guys are the best!

To all my colleagues at Klinisk Fysiologi at Karolinska University Hospital Solna who made the clinical work a delight. I would like to acknowledge **Maria Eriksson**, **Eva Maret**, **Fleming Larsen**, **Sofie Olsson**, **Raquel Themudo**, and **Peder Sörensson**. Thanks to everyone at the Department of Molecular Medicine and Surgery, for administrative help, especially **Britt-Marie Witasp**, for your help and patience when we are travelling. To **Marie Holmqvist** and **Mia Konradsdal**, for your support when teaching medical students ECG, it has been one of the most fun parts of this experience. Thanks to all the fourth semester medical students at the Karolinska University Hospital Solna, for making it effortless for me to teach. I would also like to thank all my teachers throughout the years, especially those who taught me in science class, including **Satu Koskela** and **Michael Ternander**.

To **Eman Bascal**, **Emily Westhoff**, **Ouiam Kouba**, and **Brenna Thorslund**, thanks for the best American experience I could have ever imagined when I first started doing research, and for your friendship. To **Sandra Moss**, **Rebecca Källstrand**, and **Carolina Sahlin**, for all the tacos and for always believing in me. Thanks to my dear friends from medical school, **Ann-Sofie Berger**, **Gustaf Sverin**, and **Bidisha Huq**, and not the least **Hannes Hegmar** and **Anna Hellström**, for help with everything from proof-reading texts to climbing steep mountains on our epic hikes. To **Stefanny Castaneda**, **Marielle Nilsson**, **Marilia Bognandi, Liselia Bognandi**, and everyone else from church, you are family. There are too many more to be named individually, but a big thanks to all my friends.

To my mother **Irene** and father **Fred**, for your never-ending love and support. Thanks for everything you have done, and do, for me. To my siblings, **Jolin**, **Karen**, **Lael**, and **Nathan**, you are the most fun, crazy, sweet, smart, loud, and loving bunch of people that I know. I am truly blessed to have you in my life, and I dedicate this work to you.

8 REFERENCES

1. Roth GA, Johnson C, Abajobir A, Abd-Allah F, Abera SF, Abyu G, et al. Global, Regional, and National Burden of Cardiovascular Diseases for 10 Causes, 1990 to 2015. J Am Coll Cardiol. 2017;70(1):1-25.

2. Bacharova L, Ugander M. Left ventricular hypertrophy: The relationship between the electrocardiogram and cardiovascular magnetic resonance imaging. Ann Noninvasive Electrocardiol. 2014;19(6):524-33.

3. Kors JA, van Herpen G, Sittig AC, van Bemmel JH. Reconstruction of the Frank vectorcardiogram from standard electrocardiographic leads: diagnostic comparison of different methods. Eur Heart J. 1990;11(12):1083-92.

4. Schlegel TT, Kulecz WB, Feiveson AH, Greco EC, DePalma JL, Starc V, et al. Accuracy of advanced versus strictly conventional 12-lead ECG for detection and screening of coronary artery disease, left ventricular hypertrophy and left ventricular systolic dysfunction. BMC Cardiovasc Disord. 2010;10:28.

5. Benjamin EJ, Blaha MJ, Chiuve SE, Cushman M, Das SR, Deo R, et al. Heart Disease and Stroke Statistics-2017 Update: A Report From the American Heart Association. Circulation. 2017;135(10):e146-e603.

6. Clark H. NCDs: a challenge to sustainable human development. Lancet. 2013;381(9866):510-1.

7. Kannel WB, Dawber TR, Kagan A, Revotskie N, Stokes J. Factors of risk in the development of coronary heart disease--six year follow-up experience. The Framingham Study. Ann Intern Med. 1961;55:33-50.

8. Keen H, Rose G, Pyke DA, Boyns D, Chlouverakis C. Blood-sugar and arterial disease. Lancet. 1965;2(7411):505-8.

9. Hubert HB, Feinleib M, McNamara PM, Castelli WP. Obesity as an independent risk factor for cardiovascular disease: a 26-year follow-up of participants in the Framingham Heart Study. Circulation. 1983;67(5):968-77.

10. Blair SN, Kohl HW, Paffenbarger RS, Clark DG, Cooper KH, Gibbons LW. Physical fitness and all-cause mortality. A prospective study of healthy men and women. JAMA. 1989;262(17):2395-401.

11. Mosterd A, Hoes AW. Clinical epidemiology of heart failure. Heart. 2007;93(9):1137-46.

12. Ponikowski P, Anker SD, AlHabib KF, Cowie MR, Force TL, Hu S, et al. Heart failure: preventing disease and death worldwide. ESC Heart Fail. 2014;1(1):4-25.

13. Mastandrea P. The diagnostic utility of brain natriuretic peptide in heart failure patients presenting with acute dyspnea: a meta-analysis. Clin Chem Lab Med. 2013;51(6):1155-65.

14. Yamasaki N, Kitaoka H, Matsumura Y, Furuno T, Nishinaga M, Doi Y. Heart failure in the elderly. Intern Med. 2003;42(5):383-8.

15. Criteria Committee NYHA, Inc. Diseases of the Heart and Blood Vessels. Nomenclature and Criteria for diagnosis, 6th edition. Criteria Committee, New York Heart Association , Inc. Diseases of the Heart and Blood Vessels. Nomenclature and Criteria for

diagnosis, 6th edition Boston, Little, Brown and Co. 1964, p 114: Boston, Little, Brown and Co.

1964.

16. Ponikowski P, Voors AA, Anker SD, Bueno H, Cleland JGF, Coats AJS, et al. 2016 ESC Guidelines for the diagnosis and treatment of acute and chronic heart failure: The Task Force for the diagnosis and treatment of acute and chronic heart failure of the European Society of Cardiology (ESC)Developed with the special contribution of the Heart Failure Association (HFA) of the ESC. Eur Heart J. 2016;37(27):2129-200.

17. Broberg CS, Chugh SS, Conklin C, Sahn DJ, Jerosch-Herold M. Quantification of diffuse myocardial fibrosis and its association with myocardial dysfunction in congenital heart disease. Circ Cardiovasc Imaging. 2010;3(6):727-34.

18. Moon JC, Messroghli DR, Kellman P, Piechnik SK, Robson MD, Ugander M, et al. Myocardial T1 mapping and extracellular volume quantification: a Society for Cardiovascular Magnetic Resonance (SCMR) and CMR Working Group of the European Society of Cardiology consensus statement. J Cardiovasc Magn Reson. 2013;15:92.

19. Tamarappoo BK, John BT, Reinier K, Teodorescu C, Uy-Evanado A, Gunson K, et al. Vulnerable myocardial interstitium in patients with isolated left ventricular hypertrophy and sudden cardiac death: a postmortem histological evaluation. J Am Heart Assoc. 2012;1(3):e001511.

20. Díez J, Querejeta R, López B, González A, Larman M, Martínez Ubago JL. Losartan-dependent regression of myocardial fibrosis is associated with reduction of left ventricular chamber stiffness in hypertensive patients. Circulation. 2002;105(21):2512-7.

21. McLenachan JM, Dargie HJ. Ventricular arrhythmias in hypertensive left ventricular hypertrophy. Relationship to coronary artery disease, left ventricular dysfunction, and myocardial fibrosis. Am J Hypertens. 1990;3(10):735-40.

22. Tsao CW, Gona PN, Salton CJ, Chuang ML, Levy D, Manning WJ, et al. Left Ventricular Structure and Risk of Cardiovascular Events: A Framingham Heart Study Cardiac Magnetic Resonance Study. J Am Heart Assoc. 2015;4(9):e002188.

23. Liu CY, Liu YC, Wu C, Armstrong A, Volpe GJ, van der Geest RJ, et al. Evaluation of age-related interstitial myocardial fibrosis with cardiac magnetic resonance contrast-enhanced T1 mapping: MESA (Multi-Ethnic Study of Atherosclerosis). J Am Coll Cardiol. 2013;62(14):1280-7.

24. Sundström J, Lind L, Arnlöv J, Zethelius B, Andrén B, Lithell HO. Echocardiographic and electrocardiographic diagnoses of left ventricular hypertrophy predict mortality independently of each other in a population of elderly men. Circulation. 2001;103(19):2346-51.

25. Ganau A, Devereux RB, Roman MJ, de Simone G, Pickering TG, Saba PS, et al. Patterns of left ventricular hypertrophy and geometric remodeling in essential hypertension. J Am Coll Cardiol. 1992;19(7):1550-8.

26. Lundin M, Heiberg E, Nordlund D, Gyllenhammar T, Steding-Ehrenborg K, Engblom H, et al. Mean wall thickness improved characterization and prognosis in left ventricular hypertrophy [abstract]. In: Proceedings of the 22nd Annual Meeting of the Society for Cardiovascular Magnetic Resonance; 2019, Feb 6-9; Bellevue, WA, US. Abstract ID#549719.

27. Lundin M, Heiberg E, Nordlund D, Gyllenhammar T, Steding-Ehrenborg K, Engblom H, et al. Left ventricular mass and global wall thickness - prognostic utility and characterization of left ventricular hypertrophy. *Manuscript submitted.*

28. Travers JG, Kamal FA, Robbins J, Yutzey KE, Blaxall BC. Cardiac Fibrosis: The Fibroblast Awakens. Circ Res. 2016;118(6):1021-40.

29. Hill JA. Hypertrophic reprogramming of the left ventricle: translation to the ECG. J Electrocardiol. 2012;45(6):624-9.

30. Flett AS, Hayward MP, Ashworth MT, Hansen MS, Taylor AM, Elliott PM, et al. Equilibrium contrast cardiovascular magnetic resonance for the measurement of diffuse myocardial fibrosis: preliminary validation in humans. Circulation. 2010;122(2):138-44.

31. Schelbert EB, Fridman Y, Wong TC, Abu Daya H, Piehler KM, Kadakkal A, et al. Temporal Relation Between Myocardial Fibrosis and Heart Failure With Preserved Ejection Fraction: Association With Baseline Disease Severity and Subsequent Outcome. JAMA Cardiol. 2017;2(9):995-1006.

32. Brilla CG, Rupp H, Funck R, Maisch B. The renin-angiotensin-aldosterone system and myocardial collagen matrix remodelling in congestive heart failure. Eur Heart J. 1995;16 Suppl O:107-9.

33. Aghajanian H, Kimura T, Rurik JG, Hancock AS, Leibowitz MS, Li L, et al. Targeting cardiac fibrosis with engineered T cells. Nature. 2019.

34. Miller CA, Naish JH, Bishop P, Coutts G, Clark D, Zhao S, et al. Comprehensive validation of cardiovascular magnetic resonance techniques for the assessment of myocardial extracellular volume. Circ Cardiovasc Imaging. 2013;6(3):373-83.

35. Santana LF, Cheng EP, Lederer WJ. How does the shape of the cardiac action potential control calcium signaling and contraction in the heart? J Mol Cell Cardiol. 2010;49(6):901-3.

36. Brightman MW, Reese TS. Junctions between intimately apposed cell membranes in the vertebrate brain. J Cell Biol. 1969;40(3):648-77.

37. George AL. Molecular and genetic basis of sudden cardiac death. J Clin Invest. 2013;123(1):75-83.

38. Monfredi O, Maltsev VA, Lakatta EG. Modern concepts concerning the origin of the heartbeat. Physiology (Bethesda). 2013;28(2):74-92.

39. Keith A, Flack M. The Form and Nature of the Muscular Connections between the Primary Divisions of the Vertebrate Heart. J Anat Physiol. 1907;41(Pt 3):172-89.

40. Bacharova L, Estes EH, Bang LE, Hill JA, Macfarlane PW, Rowlandson I, et al. Second statement of the working group on electrocardiographic diagnosis of left ventricular hypertrophy. J Electrocardiol. 2011;44(5):568-70.

41. Bacharova L, Szathmary V, Potse M, Mateasik A. Computer simulation of ECG manifestations of left ventricular electrical remodeling. J Electrocardiol. 2012;45(6):630-4.

42. Wang S, Ziman B, Bodi I, Rubio M, Zhou YY, D'Souza K, et al. Dilated cardiomyopathy with increased SR Ca2+ loading preceded by a hypercontractile state and diastolic failure in the alpha(1C)TG mouse. PLoS One. 2009;4(1):e4133.

43. Rossow CF, Dilly KW, Yuan C, Nieves-Cintrón M, Cabarrus JL, Santana LF. NFATc3-dependent loss of I(to) gradient across the left ventricular wall during chronic beta adrenergic stimulation. J Mol Cell Cardiol. 2009;46(2):249-56.

44. Sipido KR, Eisner D. Something old, something new: changing views on the cellular mechanisms of heart failure. Cardiovasc Res. 2005;68(2):167-74.

45. Waller AD. A Demonstration on Man of Electromotive Changes accompanying the Heart's Beat. J Physiol. 1887;8(5):229-34.

46. Einthoven W, Fahr G, De Waart A. On the direction and manifest size of the variations of potential in the human heart and on the influence of the position of the heart on the form of the electrocardiogram. Am Heart J. 1950;40(2):163-211.

47. Henson JR. Descartes and the ECG lettering series. J Hist Med Allied Sci. 1971;26(2):181-6.

48. Ershler I. Willem Einthoven--the man. The string galvanometer electrocardiograph. Arch Intern Med. 1988;148(2):453-5.

49. Koelsch S, Enge J, Jentschke S. Cardiac signatures of personality. PLoS One. 2012;7(2):e31441.

50. Fumagalli B. Unipolar value of standard limb leads; lead -VR and rational arrangement of limn leads. Am Heart J. 1954;48(2):204-23.

51. Mann H. A method of analyzing the electrocardiom. Arch Int Med; 1920;25:283-94.

52. Chou TC. When is the vectorcardiogram superior to the scalar electrocardiogram? J Am Coll Cardiol. 1986;8(4):791-9.

53. Ghista DN, Acharya UR, Nagenthiran T. Frontal plane vectorcardiograms: theory and graphics visualization of cardiac health status. J Med Syst. 2010;34(4):445-58.

54. Cortez DL, Schlegel TT. When deriving the spatial QRS-T angle from the 12-lead electrocardiogram, which transform is more Frank: regression or inverse Dower? J Electrocardiol. 2010;43(4):302-9.

55. Dower GE, Machado HB, Osborne JA. On deriving the electrocardiogram from vectoradiographic leads. Clin Cardiol. 1980;3(2):87-95.

56. Man S, Maan AC, Schalij MJ, Swenne CA. Vectorcardiographic diagnostic & prognostic information derived from the 12-lead electrocardiogram: Historical review and clinical perspective. J Electrocardiol. 2015;48(4):463-75.

57. Voulgari C, Pagoni S, Tesfaye S, Tentolouris N. The spatial QRS-T angle: implications in clinical practice. Curr Cardiol Rev. 2013;9(3):197-210.

58. Oehler A, Feldman T, Henrikson CA, Tereshchenko LG. QRS-T angle: a review. Ann Noninvasive Electrocardiol. 2014;19(6):534-42.

59. Dilaveris P, Gialafos E, Pantazis A, Synetos A, Triposkiadis F, Gialafos J. The spatial QRS-T angle as a marker of ventricular repolarisation in hypertension. J Hum Hypertens. 2001;15(1):63-70.

60. Voulgari C, Tentolouris N, Moyssakis I, Dilaveris P, Gialafos E, Papadogiannis D, et al. Spatial QRS-T angle: association with diabetes and left ventricular performance. Eur J Clin Invest. 2006;36(9):608-13.

61. Zong Y, Maanja M, Chaireti R, Schlegel TT, Ugander M, Antovic JP. Substantial prevalence of subclinical cardiovascular diseases in patients with hemophilia A evaluated by advanced electrocardiography. J Electrocardiol. 2019;58:171-5.

62. Yamazaki T, Froelicher VF, Myers J, Chun S, Wang P. Spatial QRS-T angle predicts cardiac death in a clinical population. Heart Rhythm. 2005;2(1):73-8.

63. Macfarlane PW, vanOosterom A, Pahlm O, Kligfield P, Janse M, Camm J. Comprehensive Electrocardiology. London: Springer; 2011.

64. Pipberger H, Carter T. Analysis of the normal and abnormal vectorcardiogram in its own reference frame. Circulation. 1962;25:827-40.

65. Priori SG, Mortara DW, Napolitano C, Diehl L, Paganini V, Cantù F, et al. Evaluation of the spatial aspects of T-wave complexity in the long-QT syndrome. Circulation. 1997;96(9):3006-12.

66. Okin PM, Devereux RB, Fabsitz RR, Lee ET, Galloway JM, Howard BV. Principal component analysis of the T wave and prediction of cardiovascular mortality in American Indians: the Strong Heart Study. Circulation. 2002;105(6):714-9.

67. Rautaharju PM, Kooperberg C, Larson JC, LaCroix A. Electrocardiographic predictors of incident congestive heart failure and all-cause mortality in postmenopausal women: the Women's Health Initiative. Circulation. 2006;113(4):481-9.

68. Hancock EW, Deal BJ, Mirvis DM, Okin P, Kligfield P, Gettes LS, et al. AHA/ACCF/HRS recommendations for the standardization and interpretation of the electrocardiogram: part V: electrocardiogram changes associated with cardiac chamber hypertrophy: a scientific statement from the American Heart Association Electrocardiography and Arrhythmias Committee, Council on Clinical Cardiology; the American College of Cardiology Foundation; and the Heart Rhythm Society: endorsed by the International Society for Computerized Electrocardiology. Circulation. 2009;119(10):e251-61.

69. Bacharova L, Chen H, Estes EH, Mateasik A, Bluemke DA, Lima JA, et al. Determinants of discrepancies in detection and comparison of the prognostic significance of left ventricular hypertrophy by electrocardiogram and cardiac magnetic resonance imaging. Am J Cardiol. 2015;115(4):515-22.

70. Casale PN, Devereux RB, Kligfield P, Eisenberg RR, Miller DH, Chaudhary BS, et al. Electrocardiographic detection of left ventricular hypertrophy: development and prospective validation of improved criteria. J Am Coll Cardiol. 1985;6(3):572-80.

71. Okin PM, Devereux RB, Jern S, Kjeldsen SE, Julius S, Dahlöf B. Baseline characteristics in relation to electrocardiographic left ventricular hypertrophy in hypertensive patients: the Losartan intervention for endpoint reduction (LIFE) in hypertension study. The Life Study Investigators. Hypertension. 2000;36(5):766-73.

72. Murphy ML, Thenabadu PN, de Soyza N, Meade J, Doherty JE, Baker BJ. Sensitivity of electrocardiographic criteria for left ventricular hypertrophy according to type of cardiac disease. Am J Cardiol. 1985;55(5):545-9.

73. Estes EH, Zhang ZM, Li Y, Tereschenko LG, Soliman EZ. The Romhilt-Estes left ventricular hypertrophy score and its components predict all-cause mortality in the general population. Am Heart J. 2015;170(1):104-9.

74. Bacharova L, Kyselovic J. Electrocardiographic diagnosis of left ventricular hypertrophy: is the method obsolete or should the hypothesis be reconsidered? Med Hypotheses. 2001;57(4):487-90.

75. Maanja M, Wieslander B, Schlegel TT, Bacharova L, Abu Daya H, Fridman Y, et al. Diffuse Myocardial Fibrosis Reduces Electrocardiographic Voltage Measures of Left Ventricular Hypertrophy Independent of Left Ventricular Mass. J Am Heart Assoc. 2017;6(1).

76. Mashima S. Theoretical considerations on the electrocardiogram of ventricular hypertrophy. J Electrocardiol. 1976;9(2):133-8.

77. Szathmáry V, Ruttkay-Nedecký I, Osvald R. Computer simulation of propagated activation in different types of left ventricular enlargement. Comput Methods Programs Biomed. 1994;44(2):85-91.

78. Bacharova L. Electrical and structural remodeling in left ventricular hypertrophy-a substrate for a decrease in QRS voltage? Ann Noninvasive Electrocardiol. 2007;12(3):260-73.

79. Spach MS, Heidlage JF, Dolber PC, Barr RC. Electrophysiological effects of remodeling cardiac gap junctions and cell size: experimental and model studies of normal cardiac growth. Circ Res. 2000;86(3):302-11.

80. Spach MS, Barr RC. Effects of cardiac microstructure on propagating electrical waveforms. Circ Res. 2000;86(2):E23-8.

81. Nattel S, Li D. Ionic remodeling in the heart: pathophysiological significance and new therapeutic opportunities for atrial fibrillation. Circ Res. 2000;87(6):440-7.

82. Kléber AG, Rudy Y. Basic mechanisms of cardiac impulse propagation and associated arrhythmias. Physiol Rev. 2004;84(2):431-88.

83. Petersen SE, Aung N, Sanghvi MM, Zemrak F, Fung K, Paiva JM, et al. Reference ranges for cardiac structure and function using cardiovascular magnetic resonance (CMR) in Caucasians from the UK Biobank population cohort. J Cardiovasc Magn Reson. 2017;19(1):18.

84. Karamitsos TD, Francis JM, Myerson S, Selvanayagam JB, Neubauer S. The role of cardiovascular magnetic resonance imaging in heart failure. J Am Coll Cardiol. 2009;54(15):1407-24.

85. Ramalho M, Ramalho J. Gadolinium-Based Contrast Agents: Associated Adverse Reactions. Magn Reson Imaging Clin N Am. 2017;25(4):755-64.

86. Rabi II, Zacharias JR, Millman S, Kusch P. Milestones in magnetic resonance: 'a new method of measuring nuclear magnetic moment' . 1938. J Magn Reson Imaging. 1992;2(2):131-3.

87. Bloch F. The Principle of Nuclear Induction. Science. 1953;118(3068):425-30.

88. Salerno M, Kramer CM. Advances in parametric mapping with CMR imaging. JACC Cardiovasc Imaging. 2013;6(7):806-22.

89. Ugander M, Oki AJ, Hsu LY, Kellman P, Greiser A, Aletras AH, et al. Extracellular volume imaging by magnetic resonance imaging provides insights into overt and sub-clinical myocardial pathology. Eur Heart J. 2012;33(10):1268-78.

90. Arheden H, Saeed M, Higgins CB, Gao DW, Bremerich J, Wyttenbach R, et al. Measurement of the distribution volume of gadopentetate dimeglumine at echo-planar MR imaging to quantify myocardial infarction: comparison with 99mTc-DTPA autoradiography in rats. Radiology. 1999;211(3):698-708.

91. Thygesen K, Alpert JS, Jaffe AS, Simoons ML, Chaitman BR, White HD, et al. Third universal definition of myocardial infarction. Circulation. 2012;126(16):2020-35.

92. Flachskampf FA, Schmid M, Rost C, Achenbach S, DeMaria AN, Daniel WG. Cardiac imaging after myocardial infarction. Eur Heart J. 2011;32(3):272-83.

93. Kuruvilla S, Adenaw N, Katwal AB, Lipinski MJ, Kramer CM, Salerno M. Late gadolinium enhancement on cardiac magnetic resonance predicts adverse cardiovascular outcomes in nonischemic cardiomyopathy: a systematic review and meta-analysis. Circ Cardiovasc Imaging. 2014;7(2):250-8.

94. Mahrholdt H, Wagner A, Judd RM, Sechtem U, Kim RJ. Delayed enhancement cardiovascular magnetic resonance assessment of non-ischaemic cardiomyopathies. Eur Heart J. 2005;26(15):1461-74.

95. Grothues F, Smith GC, Moon JC, Bellenger NG, Collins P, Klein HU, et al. Comparison of interstudy reproducibility of cardiovascular magnetic resonance with two-dimensional echocardiography in normal subjects and in patients with heart failure or left ventricular hypertrophy. Am J Cardiol. 2002;90(1):29-34.

96. Maceira AM, Prasad SK, Khan M, Pennell DJ. Normalized left ventricular systolic and diastolic function by steady state free precession cardiovascular magnetic resonance. J Cardiovasc Magn Reson. 2006;8(3):417-26.

97. Curtis JP, Sokol SI, Wang Y, Rathore SS, Ko DT, Jadbabaie F, et al. The association of left ventricular ejection fraction, mortality, and cause of death in stable outpatients with heart failure. J Am Coll Cardiol. 2003;42(4):736-42.

98. McDermott MM, Feinglass J, Lee PI, Mehta S, Schmitt B, Lefevre F, et al. Systolic function, readmission rates, and survival among consecutively hospitalized patients with congestive heart failure. Am Heart J. 1997;134(4):728-36.

99. Kalam K, Otahal P, Marwick TH. Prognostic implications of global LV dysfunction: a systematic review and meta-analysis of global longitudinal strain and ejection fraction. Heart. 2014;100(21):1673-80.

100. Kraigher-Krainer E, Shah AM, Gupta DK, Santos A, Claggett B, Pieske B, et al. Impaired systolic function by strain imaging in heart failure with preserved ejection fraction. J Am Coll Cardiol. 2014;63(5):447-56.

101. Armstrong AC, Gidding S, Gjesdal O, Wu C, Bluemke DA, Lima JA. LV mass assessed by echocardiography and CMR, cardiovascular outcomes, and medical practice. JACC Cardiovasc Imaging. 2012;5(8):837-48.

102. Cuspidi C, Meani S, Negri F, Giudici V, Valerio C, Sala C, et al. Indexation of left ventricular mass to body surface area and height to allometric power of 2.7: is the difference limited to obese hypertensives? J Hum Hypertens. 2009;23(11):728-34.

103. Guyon I, Elisseeff A. An introduction to variable and feature selection. *Journal of machine learning research*; 2003. p. 1157-82.

104. Galbusera F, Casaroli G, Bassani T. Artificial intelligence and machine learning in spine research. JOR Spine. 2019;2(1):e1044.

105. Kohavi R, John GH. Wrappers for feature subset selection. Artificial Intelligence; 1997;97(1-2):273-324.

106. Peduzzi P, Concato J, Feinstein AR, Holford TR. Importance of events per independent variable in proportional hazards regression analysis. II. Accuracy and precision of regression estimates. J Clin Epidemiol. 1995;48(12):1503-10.

107. AK J, RPW D, J M. Statistical pattern recognition: a review. IEEE transactions on pattern analysis and machine learning; 2000. 22(1):4-37.

108. Cohen A. Dummy Variables in Stepwise Regression. The American Statistician. 1991;45(3):226-8.

109. Gardner MJ, Altman DG. Confidence intervals rather than P values: estimation rather than hypothesis testing. Br Med J (Clin Res Ed). 1986;292(6522):746-50.

110. Machin D, Campbell MJ, Walter SJ. Medical Statistics: A Textbook for the Health Sciences. 4 ed. 2007: John Wiley & Sons, Incorporated.

111. Jorfeldt L, Pahlm O. Kliniska arbetsprov - metoder för diagnos och prognos. 2013. Studentlitteratur.

112. Lang RM, Bierig M, Devereux RB, Flachskampf FA, Foster E, Pellikka PA, et al. Recommendations for chamber quantification: a report from the American Society of Echocardiography's Guidelines and Standards Committee and the Chamber Quantification Writing Group, developed in conjunction with the European Association of Echocardiography, a branch of the European Society of Cardiology. J Am Soc Echocardiogr. 2005;18(12):1440-63.

113. Sokolow M, Lyon TP. The ventricular complex in left ventricular hypertrophy as obtained by unipolar precordial and limb leads. Am Heart J. 1949;37(2):161-86.

114. Molloy TJ, Okin PM, Devereux RB, Kligfield P. Electrocardiographic detection of left ventricular hypertrophy by the simple QRS voltage-duration product. J Am Coll Cardiol. 1992;20(5):1180-6.

115. Willems JL, Robles de Medina EO, Bernard R, Coumel P, Fisch C, Krikler D, et al. Criteria for intraventricular conduction disturbances and pre-excitation. World Health Organizational/International Society and Federation for Cardiology Task Force Ad Hoc. J Am Coll Cardiol. 1985;5(6):1261-75.

116. Badilini F, Maison Blanche P, Fayn J. Relationship between 12-lead ECG QT dispersion and 3D-ECG repolarization loop. Computers in Cardiology. 1995; 785-8.

117. Rubulis A, Jensen J, Lundahl G, Tapanainen J, Wecke L, Bergfeldt L. T vector and loop characteristics in coronary artery disease and during acute ischemia. Heart Rhythm. 2004;1(3):317-25.

118. Kellman P, Larson AC, Hsu LY, Chung YC, Simonetti OP, McVeigh ER, et al. Motion-corrected free-breathing delayed enhancement imaging of myocardial infarction. Magn Reson Med. 2005;53(1):194-200.

119. Piehler KM, Wong TC, Puntil KS, Zareba KM, Lin K, Harris DM, et al. Free-breathing, motion-corrected late gadolinium enhancement is robust and extends risk stratification to vulnerable patients. Circ Cardiovasc Imaging. 2013;6(3):423-32.

120. Wong TC, Piehler K, Meier CG, Testa SM, Klock AM, Aneizi AA, et al. Association between extracellular matrix expansion quantified by cardiovascular magnetic resonance and short-term mortality. Circulation. 2012;126(10):1206-16.

121. Wickham H, Francois R, Henry L, Müller K. Dplyr: A Grammar of Data Manipulation. 2017.

122. Wickham H. Ggplot2: Elegant Graphics for Data Analysis. Springer-Verlag New York. 2009.

123. Youden W. Index for rating diagnostic tests. Cancer. 1950;3(1):32-5.

124. DeLong ER, DeLong DM, Clarke-Pearson DL. Comparing the areas under two or more correlated receiver operating characteristic curves: a nonparametric approach. Biometrics. 1988;44(3):837-45.

125. Aro AL, Reinier K, Rusinaru C, Uy-Evanado A, Darouian N, Phan D, et al. Electrical risk score beyond the left ventricular ejection fraction: prediction of sudden cardiac death in the Oregon Sudden Unexpected Death Study and the Atherosclerosis Risk in Communities Study. Eur Heart J. 2017;38(40):3017-25.

126. White SK, Sado DM, Fontana M, Banypersad SM, Maestrini V, Flett AS, et al. T1 mapping for myocardial extracellular volume measurement by CMR: bolus only versus primed infusion technique. JACC Cardiovasc Imaging. 2013;6(9):955-62.

127. Fontana M, White SK, Banypersad SM, Sado DM, Maestrini V, Flett AS, et al. Comparison of T1 mapping techniques for ECV quantification. Histological validation and reproducibility of ShMOLLI versus multibreath-hold T1 quantification equilibrium contrast CMR. J Cardiovasc Magn Reson. 2012;14:88.

128. de Meester de Ravenstein C, Bouzin C, Lazam S, Boulif J, Amzulescu M, Melchior J, et al. Histological Validation of measurement of diffuse interstitial myocardial fibrosis by myocardial extravascular volume fraction from Modified Look-Locker imaging (MOLLI) T1 mapping at 3 T. J Cardiovasc Magn Reson. 2015;17:48.

129. aus dem Siepen F, Buss SJ, Messroghli D, Andre F, Lossnitzer D, Seitz S, et al. T1 mapping in dilated cardiomyopathy with cardiac magnetic resonance: quantification of diffuse myocardial fibrosis and comparison with endomyocardial biopsy. Eur Heart J Cardiovasc Imaging. 2015;16(2):210-6.

130. Banypersad SM, Moon JC, Whelan C, Hawkins PN, Wechalekar AD. Updates in cardiac amyloidosis: a review. J Am Heart Assoc. 2012;1(2):e000364.

131. Madias JE. Low QRS voltage and its causes. J Electrocardiol. 2008;41(6):498-500.

132. Carlsson MB, Trägårdh E, Engblom H, Hedström E, Wagner G, Pahlm O, et al. Left ventricular mass by 12-lead electrocardiogram in healthy subjects: comparison to cardiac magnetic resonance imaging. J Electrocardiol. 2006;39(1):67-72.

133. Kansal S, Roitman DI, Sheffield LT. A quantitative relationship of electrocardiographic criteria of left ventricular hypertrophy with echocardiographic left ventricular mass: a multivariate approach. Clin Cardiol. 1983;6(9):456-63.

134. Fragola PV, De Nardo D, Calò L, Cannata D. Use of the signal-averaged QRS duration for diagnosing left ventricular hypertrophy in hypertensive patients. Int J Cardiol. 1994;44(3):261-70.

135. Sjöberg S, Sundh F, Schlegel T, Maynard C, Rück A, Wagner G, et al. The relationship between electrocardiographic left ventricular hypertrophy criteria and echocardiographic mass in patients undergoing transcatheter aortic valve replacement. J Electrocardiol. 2015;48(4):630-6.

136. Okin PM, Roman MJ, Devereux RB, Pickering TG, Borer JS, Kligfield P. Time-voltage QRS area of the 12-lead electrocardiogram: detection of left ventricular hypertrophy. Hypertension. 1998;31(4):937-42.

137. Chou TC, Masangkay MP, Young R, Conway GF, Helm RA. Simple quantitative vectorcardiographic criteria for the diagnosis of right ventricular hypertrophy. Circulation. 1973;48(6):1262-7.

138. Porthan K, Virolainen J, Hiltunen TP, Viitasalo M, Väänänen H, Dabek J, et al. Relationship of electrocardiographic repolarization measures to echocardiographic left ventricular mass in men with hypertension. J Hypertens. 2007;25(9):1951-7.

139. Nowinski K, Jensen S, Lundahl G, Bergfeldt L. Changes in ventricular repolarization during percutaneous transluminal coronary angioplasty in humans assessed by QT interval, QT dispersion and T vector loop morphology. J Intern Med. 2000;248(2):126-36.

140. Kannel WB, Gordon T, Castelli WP, Margolis JR. Electrocardiographic left ventricular hypertrophy and risk of coronary heart disease. The Framingham study. Ann Intern Med. 1970;72(6):813-22.

141. Varriale P, Alfenito JC, Kennedy RJ. The vectorcardiogram of left ventricular hypertrophy. Analysis and criteria (Frank Lead system). Circulation. 1966;33(4):569-76.

142. Romhilt DW, Greenfield JC, Estes EH. Vectorcardiographic diagnosis of left ventricular hypertrophy. Circulation. 1968;37(1):15-9.

143. Maanja M, Schlegel TT, Kozor R, Lundin M, Wieslander B, Wong TC, et al. The electrical determinants of increased wall thickness and mass in left ventricular hypertrophy. J Electrocardiol. 2019;58:80-6.

144. Bacharova L, Estes EH. Left Ventricular Hypertrophy by the Surface ECG. J Electrocardiol. 2017;50(6):906-8.

145. Bacharova L, Estes EH, Hill JA, Pahlm O, Schillaci G, Strauss D, et al. Changing role of ECG in the evaluation left ventricular hypertrophy. J Electrocardiol. 2012;45(6):609-11.

146. Cortez D, Sharma N, Devers C, Devers E, Schlegel TT. Visual transform applications for estimating the spatial QRS-T angle from the conventional 12-lead ECG: Kors is still most Frank. J Electrocardiol. 2014;47(1):12-9.

147. Man S, Rahmattulla C, Maan AC, Holman E, Bax JJ, van der Wall EE, et al. Role of the vectorcardiogram-derived spatial QRS-T angle in diagnosing left ventricular hypertrophy. J Electrocardiol. 2012;45(2):154-60.

148. Bazett, HC. An analysis of the time-relations of electrocardiograms. Heart. 1920; 7:353.

149. Montanez A, Ruskin JN, Hebert PR, Lamas GA, Hennekens CH. Prolonged QTc interval and risks of total and cardiovascular mortality and sudden death in the general population: a review and qualitative overview of the prospective cohort studies. Arch Intern Med. 2004;164(9):943-8.

150. Stanton T, Leano R, Marwick TH. Prediction of all-cause mortality from global longitudinal speckle strain: comparison with ejection fraction and wall motion scoring. Circ Cardiovasc Imaging. 2009;2(5):356-64.

151. Dastidar AG, Baritussio A, De Garate E, Drobni Z, Biglino G, Singhal P, et al. Prognostic Role of Cardiac MRI and Conventional Risk Factors in Myocardial Infarction With Nonobstructed Coronary Arteries. JACC Cardiovasc Imaging. 2019.